Available online at www.sciencedirect.com
ScienceDirect
European Journal of Mechanics B/Fluids 26 (2007) 155–181

Gas separation by means of the Knudsen compressor

Shigeru Takata [a,*], Hiroshi Sugimoto [b], Shingo Kosuge [c,1]

[a] *Department of Mechanical Engineering and Science and Advanced Research Institute of Fluid Science and Engineering, Graduate School of Engineering, Kyoto University, Kyoto 606-8501, Japan*
[b] *Department of Aeronautics and Astronautics and Advanced Research Institute of Fluid Science and Engineering, Graduate School of Engineering, Kyoto University, Kyoto 606-8501, Japan*
[c] *Laboratoire MIP, Université Paul Sabatier, 118, route de Narbonne, 31062 Toulouse Cedex 4, France*

Received 17 November 2005; accepted 2 May 2006

Available online 3 July 2006

Abstract

A possibility of making use of the Knudsen compressor as a gas separator is investigated. Starting from the description at the microscopic level on the basis of the kinetic theory of gases, a fluid-dynamic model describing the behaviour of the mixture in the Knudsen compressor is derived. Then, by the use of this model, it is numerically demonstrated that the Knudsen compressor works certainly as a gas separator. The separation performance is shown to reach a practical level by increasing the number of elemental units in the device. The numerical simulation is carried out for various molecular models, not only for fundamental models, the hard-sphere and Maxwell molecules, but also for more realistic models such as the inverse power-law potential and Lennard-Jones models, assuming the McCormack model equation at the microscopic level. The results show that the modelling by the celebrated Maxwell molecule (or the BGK-type model equation) fails to capture the phenomenon of the gas separation in the device. This presents a remarkable contrast to the capability of the other fundamental model, the hard-sphere molecule, even though this model exaggerates the phenomenon to some extent.

PACS: 51.10.+y; 47.45.-n; 47.70.Nd; 05.20.Dd

Keywords: Gas separation; Binary mixture; Boltzmann equation; Kinetic theory of gases; Knudsen compressor; Knudsen gas; Poiseuille flow; Thermal transpiration; Concentration-driven flow

1. Introduction

Recent development of the micro-device engineering requires the precise description of gas flows in microscale systems. In microscale systems, the mean free path of gas molecules is comparable to the system scale, so that the gas in the system is no longer in a local equilibrium state and its behaviour cannot be described correctly by the

* Corresponding author.
E-mail address: takata@aero.mbox.media.kyoto-u.ac.jp (S. Takata).
[1] Permanent address: Department of Mechanical Engineering and Science and Advanced Research Institute of Fluid Science and Engineering, Graduate School of Engineering, Kyoto University, Kyoto 606-8501, Japan.

0997-7546/$ – see front matter
doi:10.1016/j.euromechflu.2006.05.002

conventional gas dynamics. The description on the basis of the kinetic theory (the Boltzmann system), which has been developed mainly aiming at the study of gas flows at low pressures, is inevitable.

One of the most classical but important findings by the kinetic theory is that a steady gas flow can be induced by a thermal effect even without external forces at low pressures or in microscale systems. The representative example of such flow is the *thermal transpiration* [1–3]. This is a flow induced in a channel (or a pipe) with a gradient of temperature along its surface. This phenomenon of low pressure gases (or gases in microscale systems) suggests that, by connecting two tanks with a very fine tube with a gradient of temperature, one can transport a certain amount of gas from one to the other. That is, the fine tube with a temperature gradient has a pumping effect. However, in order to increase the effect, it is required to give a steeper gradient of temperature or to make the tube longer. Both requirements lead to an unlimitedly large difference of temperature in the tube, yielding a severe limitation for the practical use of this simple device.

As early as 1910, an improvement of the above simple idea was proposed by Knudsen [2]. In place of a simple tube with a temperature gradient, Knudsen made a device of periodic structure, which is nowadays called the *Knudsen compressor*. It is a series of the connection of a narrow and a thick glass tube, equipped with a heater at every other junction. By using this device, he achieved the pressure difference of about 10 by experiment, avoiding the unlimited increase of temperature in the device. However, his pioneering work has not been paid attention to for a long time. It is only in the middle of 90's that the modern kinetic researches on the thermally-driven pump were initiated by the rediscovery of the Knudsen compressor [4,5]. Since then, the Knudsen compressor and its variants have been intensively studied (e.g., Refs. [6–10] and the references in the next paragraph) mainly in two research groups, the groups in Kyoto and in Los Angeles.

In Kyoto group, since Ref. [5], the pumps making use of the kinetic thermal effect have been studied both theoretically and experimentally [11–18]. The prototype of the Knudsen compressor proposed by this group is shown in Fig. 1. In Refs. [13,19], the Knudsen compressor with the narrow tube being replaced by the thick one with shelves is shown to have a pumping effect too. The prototype in the figure is the improved version of the Knudsen compressor aiming at the synergistic effect of two types of geometry. In the same group, a new type of thermally-driven pump making use of the *thermal edge flow* [20,21] was invented recently by Sugimoto and Sone [17] (the *thermal edge pump*). In the meantime, a new theoretical approach to the study of thermal pumps was proposed by Aoki and Degond [16], in which a diffusive fluid-dynamic model is derived for the description of the gas behaviour in the Knudsen compressor. Although the analysis in this reference is carried out by the use of a simplified BGK-type relaxation model, the extension to the original Boltzmann system is also possible [18].

In viewing the literature on the Knudsen compressor and its variants, it would appear that the studies done so far aim at the research of pumping effect and the analyses were naturally limited to the case of a single-species gas. As a matter of course, the same pumping effect is observed for a gas mixture. However, if one thinks of this case a little carefully, one would notice a new interesting possibility of the devices. It is a possibility as a gas separator. Recently Kosuge, Sato, Takata and Aoki [22] carried out accurate numerical analyses of three elemental flows of a binary gas mixture in a two-dimensional channel, i.e., the pressure-gradient-driven flow (Poiseuille flow), the temperature-gradient-driven flow (thermal transpiration) and the concentration-gradient-driven flow, on the basis of the original Boltzmann equation for hard-sphere molecules and clarified the comprehensive feature of the flows for a wide range of the Knudsen numbers. Observation of the results, as well as those in the references in Ref. [22], shows that the

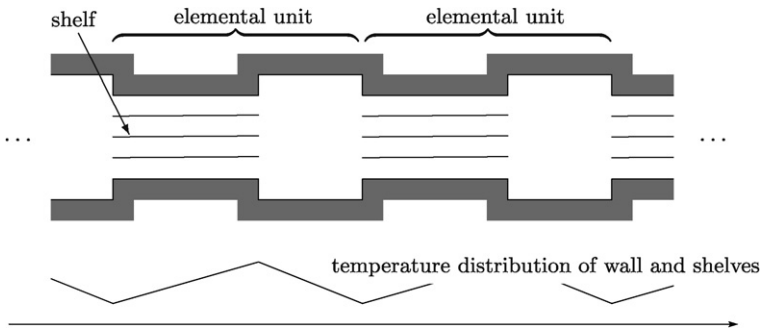

Fig. 1. Conceptual schematic of the prototype Knudsen compressor.

particle flux of each species is different from each other in rarefied gas regime, so is the transport rate of each species. This means, as is explicitly mentioned in Sharipov and Kalempa [23], that at the outlet one can take a mixture of different composition from that at the inlet. Motivated by this observation, in the present work, we shall investigate the possibility of the Knudsen compressor as a gas separator. We shall employ here the approach proposed by Aoki and Degond [16,18]. Recently, we found a patent [24] about the idea of the device designed for the compression and separation of gases, which is essentially the same as the Knudsen compressor. However, the present work would be the first quantitative study on the performance of the Knudsen compressor as a gas separator.

The paper is organized as follows. Following the recipe in Ref. [16], we first consider in Section 2 the mixture in a straight two-dimensional channel of uniform width, formulate the problem at the microscopic level on the basis of the kinetic theory of gases and derive a fluid-dynamic model for the description of the mixture in this channel. Then in Section 3 we consider the junction problem of the channels of different widths and derive the connection condition at the junction for the fluid-dynamic model. With the aid of the results in these sections, we present in Section 4 the fluid-dynamic model for the Knudsen compressor. We demonstrate the performance of the device as a gas separator by numerical simulations of this model in Section 5.

2. Fluid-dynamic model in a straight two-dimensional channel of uniform width

2.1. Problem and assumption

Consider a binary mixture of two-species gases, say species A and species B, in a straight two-dimensional channel of uniform width oriented to the direction of X_1, where X_i's are the Cartesian space coordinates (Fig. 2). The side walls of the channel are separated by a distance D and are located at $X_2 = \pm D/2$. The temperatures of the walls may vary along the channel, i.e., in the direction of X_1, but are constant both in time t and in coordinate X_3. They are supposed to take a common value at the same location in X_1 and will be denoted by $T_w(X_1)$. There is no external force. We will investigate the behaviour of the mixture in the channel by assuming that

(i) The behaviour of the mixture can be described by the Boltzmann equation for binary gas mixtures.
(ii) The gas molecules are reflected diffusely on the surface of the walls.
(iii) The characteristic length of the variation of the wall temperature, L, is much larger than the separation distance of the walls (the width of channel), D.

Before preceding further, we shall make two remarks on the assumptions above. Firstly, since we consider the problem by the use of the Boltzmann system, the mean free path of a molecule ℓ is supposed to be comparable to the separation distance of the walls D, i.e., $\ell \sim D$. Secondly, because of the assumption (iii), the state of the mixture would vary in the scale of L, not of D, in the direction of X_1. As a result, since $\ell \sim D \ll L$, the molecules undergo innumerable collisions with both other molecules and the walls when travelling in that direction until its surroundings change meaningfully. This is the clue idea in deriving the fluid-dynamic model in Section 2 (see also, for example, Refs. [25–29]).

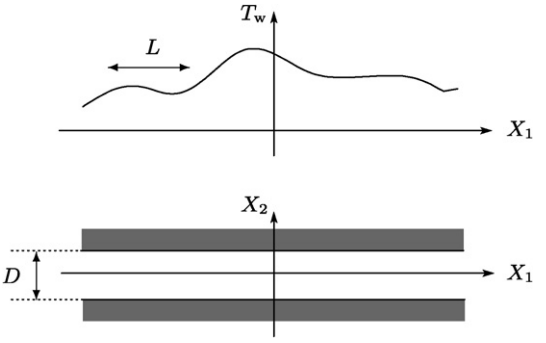

Fig. 2. Schematic of the straight two-dimensional channel of uniform width.

2.2. Basic equations and boundary conditions

Let us denote by $\boldsymbol{\xi} = (\xi_1, \xi_2, \xi_3)$ the molecular velocity and by $f^\alpha(t, \boldsymbol{X}, \boldsymbol{\xi})$ the velocity distribution function of molecules of α-species gas ($\alpha = \mathrm{A}, \mathrm{B}$). In the sequel, the Greek letters α and β will be symbolically used to denote the gas species, i.e., $\{\alpha, \beta\} = \{\mathrm{A}, \mathrm{B}\}$. Then, in the present problem, the Boltzmann equation and the boundary condition on the side walls can be written as

$$\frac{\partial f^\alpha}{\partial t} + \xi_1 \frac{\partial f^\alpha}{\partial X_1} + \xi_2 \frac{\partial f^\alpha}{\partial X_2} = J^{\mathrm{B}\alpha}\big(f^{\mathrm{B}}, f^\alpha\big) + J^{\mathrm{A}\alpha}\big(f^{\mathrm{A}}, f^\alpha\big), \tag{1a}$$

$$f^\alpha = \sigma_{2\pm}\left(f^\alpha(\boldsymbol{\xi}); \frac{m^\alpha}{2kT_{\mathrm{w}}}\right) M\left(\boldsymbol{\xi}; \frac{m^\alpha}{2kT_{\mathrm{w}}}\right), \quad \xi_2 \lessgtr 0, \ X_2 = \pm\frac{D}{2}, \tag{1b}$$

where m^α is the mass of a molecule of species α, k the Boltzmann constant, $\sigma_{2\pm}$ a constant (in $\boldsymbol{\xi}$) depending on the arguments defined by

$$\sigma_{i\pm}\big(f(\boldsymbol{\xi}); a\big) = \pm 2(\pi a)^{1/2} \int\limits_{\xi_i \gtrless 0} \xi_i f(\boldsymbol{\xi})\, \mathrm{d}^3\xi \quad (i = 1, 2),$$

with $\mathrm{d}^3\xi = \mathrm{d}\xi_1\, \mathrm{d}\xi_2\, \mathrm{d}\xi_3$ and M the normalized Maxwellian given by

$$M(\boldsymbol{\xi}; a) = \left(\frac{a}{\pi}\right)^{3/2} \exp\big(-a|\boldsymbol{\xi}|^2\big).$$

In Eq. (1b), the argument $\boldsymbol{\xi}$ of f^α is explicitly shown in order to indicate the variable of integration in the definition of $\sigma_{2\pm}$, while the other arguments t, X_1 and X_2 are suppressed for conciseness. We shall follow this convention in the sequel. $J^{\beta\alpha}$'s in Eq. (1a) are the collision integrals defined by

$$J^{\beta\alpha}(f, g) = \int (f'_* g' - f_* g) B^{\beta\alpha}\left(\frac{|\boldsymbol{e}\cdot\boldsymbol{V}|}{|\boldsymbol{V}|}, |\boldsymbol{V}|\right) \mathrm{d}\Omega(\boldsymbol{e})\, \mathrm{d}^3\xi_*, \tag{2a}$$

$$f'_* = f(\boldsymbol{\xi}'_*), \quad g' = g(\boldsymbol{\xi}'), \quad f_* = f(\boldsymbol{\xi}_*), \quad g = g(\boldsymbol{\xi}), \tag{2b}$$

$$\boldsymbol{\xi}' = \boldsymbol{\xi} + \frac{\mu^{\beta\alpha}}{m^\alpha}(\boldsymbol{e}\cdot\boldsymbol{V})\boldsymbol{e}, \qquad \boldsymbol{\xi}'_* = \boldsymbol{\xi}_* - \frac{\mu^{\beta\alpha}}{m^\beta}(\boldsymbol{e}\cdot\boldsymbol{V})\boldsymbol{e}, \tag{2c}$$

$$\mu^{\beta\alpha} = \frac{2m^\alpha m^\beta}{m^\alpha + m^\beta}, \qquad \boldsymbol{V} = \boldsymbol{\xi}_* - \boldsymbol{\xi}, \tag{2d}$$

where $\boldsymbol{e}$ is a unit vector, $\mathrm{d}\Omega(\boldsymbol{e})$ the solid angle element in the direction of $\boldsymbol{e}$ and $\mathrm{d}^3\xi_* = \mathrm{d}\xi_{*1}\, \mathrm{d}\xi_{*2}\, \mathrm{d}\xi_{*3}$. $B^{\beta\alpha}$ is a non-negative function of its arguments whose functional form is determined by the molecular interaction between species β and α. It has the symmetry property of $B^{\mathrm{BA}} = B^{\mathrm{AB}}$ because of the law of action and reaction. The integration in Eq. (2a) is carried out over the all directions of $\boldsymbol{e}$ and over the whole space of $\boldsymbol{\xi}_*$. The initial- and boundary-value problem for the binary gas mixture in the channel is formulated by Eq. (1) supplemented by an initial condition.

For the later convenience, we introduce some macroscopic quantities. The molecular number density n^α, mass density ρ^α, flow velocity $\boldsymbol{v}^\alpha = (v_1^\alpha, v_2^\alpha, 0)$, pressure p^α and temperature T^α of α-species gas are defined as

$$n^\alpha = \int f^\alpha\, \mathrm{d}^3\xi, \quad \rho^\alpha = m^\alpha n^\alpha, \quad n^\alpha v_i^\alpha = \int \xi_i f^\alpha\, \mathrm{d}^3\xi \quad (i = 1, 2), \tag{3}$$

$$p^\alpha = n^\alpha k T^\alpha = \frac{1}{3}\int \big|\boldsymbol{\xi} - \boldsymbol{v}^\alpha\big|^2 m^\alpha f^\alpha\, \mathrm{d}^3\xi, \tag{4}$$

where, and in the sequel unless otherwise stated, the domain of integration is the whole space of $\boldsymbol{\xi}$ (or of the variable of integration). The counterparts of the mixture, i.e., the molecular number density n, mass density ρ, mass average velocity $\boldsymbol{v} = (v_1, v_2, 0)$, pressure p and temperature T, are expressed by a proper combination of the quantities above as

$$n = n^{\mathrm{A}} + n^{\mathrm{B}}, \quad \rho = \rho^{\mathrm{A}} + \rho^{\mathrm{B}}, \quad \rho\boldsymbol{v} = \rho^{\mathrm{A}}\boldsymbol{v}^{\mathrm{A}} + \rho^{\mathrm{B}}\boldsymbol{v}^{\mathrm{B}}, \tag{5}$$

$$p = nkT = \sum_{\alpha=\mathrm{A},\mathrm{B}} \left(p^\alpha + \frac{1}{3}\rho^\alpha \big|\boldsymbol{v} - \boldsymbol{v}^\alpha\big|^2\right). \tag{6}$$

In the sequel, we also use the concentration (or the molar fraction) χ^α of α-species gas defined by

$$\chi^\alpha = n^\alpha/n. \tag{7}$$

Note that $\chi^{\mathrm{A}} + \chi^{\mathrm{B}} = 1$ by definition.

2.3. Scaling and dimensionless description

As is briefly described at the end of Section 2.1, the state of the mixture is expected to vary in the X_1-direction in the scale of L, while it varies in much smaller scale, the scale of D, in the X_2-direction, because of the assumption (iii). We shall consider such a solution of the Boltzmann system (1). We start with the physical discussions on the estimate of the time scale of variation.

In the present situation, the behaviour of the solution is expected to be well described fluid-dynamically in the direction of X_1, because $L \gg D \sim \ell$, i.e., $\ell/L \ll 1$. The Mach number of the flow Ma thermally induced by the kinetic effect is of $\mathrm{O}(\ell/L)$. Therefore it is natural to take the quantity L^2/cD with c being the sound speed as the time scale of variation because of the relation

$$\text{time scale} = \frac{\text{characteristic length}}{\text{representative flow speed}} = \frac{L}{c\,Ma} = \mathrm{O}\left(\frac{L^2}{c\,\ell}\right) \sim \mathrm{O}\left(\frac{L^2}{c\,D}\right).$$

It should be noted that the Mach number of $\mathrm{O}(\ell/L)$ implies the Reynolds number is of $\mathrm{O}(1)$ because of the so-called von Karman relation [30,19] $Ma \sim Re\,Kn$, where $Kn = \ell/L$ and Re is the Reynolds number.

Keeping in mind the estimate above, we introduce the following dimensionless variables:

$$\begin{aligned}
&s = t/t_*, \quad x_1 = X_1/L, \quad x_2 = X_2/D_*, \quad \boldsymbol{\zeta} = \boldsymbol{\xi}/\big(2kT_*/m^{\mathrm{A}}\big)^{1/2},\\
&\hat{f}^\alpha = f^\alpha/\big[n_*\big(2kT_*/m^{\mathrm{A}}\big)^{-3/2}\big], \qquad \big(\hat{n}^\alpha, \hat{n}\big) = \big(n^\alpha, n\big)/n_*,\\
&\big(\hat{\rho}^\alpha, \hat{\rho}\big) = \big(\rho^\alpha, \rho\big)/n_* m^{\mathrm{A}}, \qquad \big(\hat{\boldsymbol{v}}^\alpha, \hat{\boldsymbol{v}}\big) = \big(\boldsymbol{v}^\alpha, \boldsymbol{v}\big)/\big(2kT_*/m^{\mathrm{A}}\big)^{1/2},\\
&\big(\hat{p}^\alpha, \hat{p}\big) = \big(p^\alpha, p\big)/p_*, \quad \big(\widehat{T}^\alpha, \widehat{T}\big) = \big(T^\alpha, T\big)/T_*, \quad \widehat{T}_{\mathrm{w}} = T_{\mathrm{w}}/T_*,
\end{aligned}$$

where n_* is the reference molecular number density, T_* the reference temperature, p_* the reference pressure defined by $p_* = n_* k T_*$ and

$$t_* = \frac{L^2}{(2kT_*/m^{\mathrm{A}})^{1/2} D_*}.$$

The references n_* and T_* are to be chosen in a certain proper manner. In the above, the coordinate X_2 is made dimensionless by the factor D_* instead of D itself. The former is different from the latter by a factor of a, i.e., $a = D/D_*$, that is supposed to be a positive constant of $\mathrm{O}(1)$. This choice of reference length is simply for the convenience of the later discussions on the connection of channels of different widths. For the time being, if prefer, one may put $D_* = D$ or $a = 1$. Further, we introduce the following dimensionless quantities:

$$\epsilon = D_*/L, \quad \widehat{m}^\alpha = m^\alpha/m^{\mathrm{A}}, \quad K^{\beta\alpha} = B_*^{\beta\alpha}/B_*^{\mathrm{AA}}, \quad \mathrm{K}_* = \ell_*/D_*,$$

where

$$\ell_* = \frac{1}{n_* B_*^{\mathrm{AA}}}\sqrt{\frac{2kT_*}{m^{\mathrm{A}}}}, \tag{8}$$

$$B_*^{\beta\alpha} = \frac{\sqrt{\pi}}{2}\int M\left(\boldsymbol{\xi}_*; \frac{m^\beta}{2kT_*}\right) M\left(\boldsymbol{\xi}; \frac{m^\alpha}{2kT_*}\right) B^{\beta\alpha}\left(\frac{|\boldsymbol{e}\cdot\boldsymbol{V}|}{|\boldsymbol{V}|}, |\boldsymbol{V}|\right) \mathrm{d}\Omega(\boldsymbol{e})\,\mathrm{d}^3\xi_*\,\mathrm{d}^3\xi. \tag{9}$$

Here ℓ_* is the reference mean free path of a molecule and K_* is the corresponding reference Knudsen number.

With the dimensionless quantities introduced above, the original Boltzmann system is reformulated as

$$\epsilon^2 \partial_s \hat{f}^\alpha + \epsilon\,\zeta_1 \partial_{x_1} \hat{f}^\alpha + \zeta_2 \partial_{x_2} \hat{f}^\alpha = \frac{1}{\mathrm{K}_*} \sum_{\beta=\mathrm{A},\mathrm{B}} K^{\beta\alpha}\,\hat{J}^{\beta\alpha}\big(\hat{f}^\beta, \hat{f}^\alpha\big), \tag{10a}$$

$$\hat{f}^\alpha = \sigma_{2\pm}\left(\hat{f}^\alpha(\boldsymbol{\zeta}); \frac{\widehat{m}^\alpha}{\widehat{T}_{\mathrm{w}}}\right) M\left(\boldsymbol{\zeta}; \frac{\widehat{m}^\alpha}{\widehat{T}_{\mathrm{w}}}\right), \quad \zeta_2 \lessgtr 0,\ x_2 = \pm\frac{a}{2}, \tag{10b}$$

where

$$\hat{J}^{\beta\alpha}(f,g)=\int (f'_*g'-f_*g)b^{\beta\alpha}\left(\frac{|\boldsymbol{e}\cdot\widehat{\boldsymbol{V}}|}{|\widehat{\boldsymbol{V}}|},|\widehat{\boldsymbol{V}}|\right)\mathrm{d}\Omega(\boldsymbol{e})\,\mathrm{d}^3\boldsymbol{\zeta}_*, \tag{11a}$$

$$f'_*=f(\boldsymbol{\zeta}'_*),\quad g'=g(\boldsymbol{\zeta}'),\quad f_*=f(\boldsymbol{\zeta}_*),\quad g=g(\boldsymbol{\zeta}), \tag{11b}$$

$$\boldsymbol{\zeta}'=\boldsymbol{\zeta}+\frac{\hat{\mu}^{\beta\alpha}}{\widehat{m}^{\alpha}}(\boldsymbol{e}\cdot\widehat{\boldsymbol{V}})\boldsymbol{e},\qquad \boldsymbol{\zeta}'_*=\boldsymbol{\zeta}_*-\frac{\hat{\mu}^{\beta\alpha}}{\widehat{m}^{\beta}}(\boldsymbol{e}\cdot\widehat{\boldsymbol{V}})\boldsymbol{e}, \tag{11c}$$

$$\hat{\mu}^{\beta\alpha}=\frac{2\widehat{m}^{\alpha}\widehat{m}^{\beta}}{\widehat{m}^{\alpha}+\widehat{m}^{\beta}},\quad \widehat{\boldsymbol{V}}=\boldsymbol{\zeta}_*-\boldsymbol{\zeta},\quad b^{\beta\alpha}=\frac{B^{\beta\alpha}}{B_*^{\beta\alpha}}. \tag{11d}$$

Here again, the system (10) must be supplemented by a dimensionless initial condition. The definitions of the macroscopic quantities (3)–(7) are transformed into the following:

$$\hat{n}^{\alpha}=\int \hat{f}^{\alpha}\,\mathrm{d}^3\boldsymbol{\zeta},\quad \hat{\rho}^{\alpha}=\widehat{m}^{\alpha}\hat{n}^{\alpha},\quad \hat{n}^{\alpha}\hat{v}_i^{\alpha}=\int \zeta_i\hat{f}^{\alpha}\,\mathrm{d}^3\boldsymbol{\zeta}\quad (i=1,2), \tag{12}$$

$$\hat{p}^{\alpha}=\hat{n}^{\alpha}\widehat{T}^{\alpha}=\frac{2}{3}\int\left|\boldsymbol{\zeta}-\hat{\boldsymbol{v}}^{\alpha}\right|^2\widehat{m}^{\alpha}\hat{f}^{\alpha}\,\mathrm{d}^3\boldsymbol{\zeta}, \tag{13}$$

and

$$\hat{n}=\hat{n}^{\mathrm{A}}+\hat{n}^{\mathrm{B}},\quad \hat{\rho}=\hat{\rho}^{\mathrm{A}}+\hat{\rho}^{\mathrm{B}},\quad \chi^{\alpha}=\hat{n}^{\alpha}/\hat{n}, \tag{14}$$

$$\hat{\rho}\hat{\boldsymbol{v}}=\hat{\rho}^{\mathrm{A}}\hat{\boldsymbol{v}}^{\mathrm{A}}+\hat{\rho}^{\mathrm{B}}\hat{\boldsymbol{v}}^{\mathrm{B}},\quad \hat{p}=\hat{n}\widehat{T}=\sum_{\alpha=\mathrm{A,B}}\left(\hat{p}^{\alpha}+\frac{2}{3}\hat{\rho}^{\alpha}\left|\hat{\boldsymbol{v}}^{\alpha}-\hat{\boldsymbol{v}}\right|^2\right). \tag{15}$$

It should be noted that ϵ is a small parameter from the assumption (iii) in Section 2.1 and that it arises in the first two terms of the left-hand side of the scaled Boltzmann equation (10a). We shall seek the solution of the system (10) in a power series of ϵ in the next subsection.

Remark 1. The integral in the right-hand side of Eq. (9) does not remain finite in general. In the case, in the dimensionless formulation, in place of $B_*^{\beta\alpha}$'s defined by Eq. (9), one should use as $B_*^{\beta\alpha}$'s those constants that are chosen properly and satisfy the symmetry property $B_*^{\mathrm{AB}}=B_*^{\mathrm{BA}}$. See Appendices A.2.2–A.2.4 for specific examples.

2.4. Asymptotic analysis and fluid-dynamic model

In the present section, aiming at deriving the fluid-dynamic model for the flow of gas mixtures in the channel, we shall seek the solution $\hat{f}^{\alpha}$ to the system (10) in a power series of ϵ:

$$\hat{f}^{\alpha}=\hat{f}^{\alpha}_{(0)}+\hat{f}^{\alpha}_{(1)}\epsilon+\cdots.$$

Substituting this expansion into the system (10) and equating like powers of ϵ lead to a series of boundary-value problems for $\hat{f}^{\alpha}_{(0)},\hat{f}^{\alpha}_{(1)},\ldots$:

$\underline{\mathrm{O}(\epsilon^0)}$

$$\zeta_2\partial_{x_2}\hat{f}^{\alpha}_{(0)}=\frac{1}{\mathrm{K}_*}\sum_{\beta=\mathrm{A,B}}K^{\beta\alpha}\hat{J}^{\beta\alpha}\big(\hat{f}^{\beta}_{(0)},\hat{f}^{\alpha}_{(0)}\big), \tag{16a}$$

$$\hat{f}^{\alpha}_{(0)}=\sigma_{2\pm}\left(\hat{f}^{\alpha}_{(0)}(\boldsymbol{\zeta});\frac{\widehat{m}^{\alpha}}{\widehat{T}_{\mathrm{w}}}\right)M\left(\boldsymbol{\zeta};\frac{\widehat{m}^{\alpha}}{\widehat{T}_{\mathrm{w}}}\right),\quad \zeta_2\lessgtr 0,\ x_2=\pm\frac{a}{2}, \tag{16b}$$

$\underline{\mathrm{O}(\epsilon^1)}$

$$\zeta_1\partial_{x_1}\hat{f}^{\alpha}_{(0)}+\zeta_2\partial_{x_2}\hat{f}^{\alpha}_{(1)}=\frac{1}{\mathrm{K}_*}\sum_{\beta=\mathrm{A,B}}K^{\beta\alpha}\big[\hat{J}^{\beta\alpha}\big(\hat{f}^{\beta}_{(0)},\hat{f}^{\alpha}_{(1)}\big)+\hat{J}^{\beta\alpha}\big(\hat{f}^{\beta}_{(1)},\hat{f}^{\alpha}_{(0)}\big)\big], \tag{17a}$$

$$\hat{f}^{\alpha}_{(1)}=\sigma_{2\pm}\left(\hat{f}^{\alpha}_{(1)}(\boldsymbol{\zeta});\frac{\widehat{m}^{\alpha}}{\widehat{T}_{\mathrm{w}}}\right)M\left(\boldsymbol{\zeta};\frac{\widehat{m}^{\alpha}}{\widehat{T}_{\mathrm{w}}}\right),\quad \zeta_2\lessgtr 0,\ x_2=\pm\frac{a}{2}, \tag{17b}$$

$\underline{\mathrm{O}(\epsilon^2)}$

$$\partial_s \hat{f}^\alpha_{(0)} + \zeta_1 \partial_{x_1} \hat{f}^\alpha_{(1)} + \zeta_2 \partial_{x_2} \hat{f}^\alpha_{(2)} = \frac{1}{\mathrm{K}_*} \sum_{\beta=\mathrm{A,B}} K^{\beta\alpha}\big[\hat{J}^{\beta\alpha}\big(\hat{f}^\beta_{(0)}, \hat{f}^\alpha_{(2)}\big) + \hat{J}^{\beta\alpha}\big(\hat{f}^\beta_{(2)}, \hat{f}^\alpha_{(0)}\big) + \hat{J}^{\beta\alpha}\big(\hat{f}^\beta_{(1)}, \hat{f}^\alpha_{(1)}\big)\big], \tag{18a}$$

$$\hat{f}^\alpha_{(2)} = \sigma_{2\pm}\left(\hat{f}^\alpha_{(2)}(\boldsymbol{\zeta}); \frac{\widehat{m}^\alpha}{\widehat{T}_\mathrm{w}}\right) M\left(\boldsymbol{\zeta}; \frac{\widehat{m}^\alpha}{\widehat{T}_\mathrm{w}}\right), \quad \zeta_2 \lessgtr 0,\ x_2 = \pm\frac{a}{2}, \tag{18b}$$

and so on. This series of problems can be solved from the lowest order.

Corresponding to the expansion of $\hat{f}^\alpha$, we expand the macroscopic quantities as

$$\hat{n}^\alpha = \hat{n}^\alpha_{(0)} + \hat{n}^\alpha_{(1)}\epsilon + \cdots, \qquad \widehat{T}^\alpha = \widehat{T}^\alpha_{(0)} + \widehat{T}^\alpha_{(1)}\epsilon + \cdots, \quad \text{etc.}$$

The expressions of the coefficient functions $\hat{n}^\alpha_{(0)}$, $\hat{n}^\alpha_{(1)}$, $\widehat{T}^\alpha_{(0)}$, $\widehat{T}^\alpha_{(1)}$, etc. in terms of $\hat{f}^\alpha_{(0)}$, $\hat{f}^\alpha_{(1)}$, etc. are obtained by substituting the expansions into Eqs. (3)–(7) and by equating like powers of ϵ. We omit these expressions for conciseness.

Remark 2. The original initial- and boundary-value problem is reduced to a series of boundary-value problems. Consequently, as will be shown in Section 2.4.1, $\hat{f}^\alpha_{(0)}$ is the bi-Maxwellian given by Eq. (19), and thus the initial data must be of this form . This is due to the time scaling introduced in Section 2.3. If the initial data of different form are given, they evolve into the bi-Maxwellian in a very short time of $\mathrm{O}(\epsilon^2)$, with keeping the number densities of individual species averaged in each cross section unchanged. The present analysis is intended to study the evolution after this initial short-time period.

2.4.1. The solution $\hat{f}^\alpha_{(0)}$ of the problem (16)

The system (16) is a boundary-value problem for $\hat{f}^\alpha_{(0)}$, in which s and x_1 occur as parameters. The solution $\hat{f}^\alpha_{(0)}$ of this problem can be shown to be the following bi-Maxwellian independent of x_2:

$$\hat{f}^\alpha_{(0)} = \hat{n}^\alpha_{(0)}(s, x_1) M\left(\boldsymbol{\zeta}; \frac{\widehat{m}^\alpha}{\widehat{T}_\mathrm{w}(x_1)}\right) = \frac{\hat{n}^\alpha_{(0)}(s, x_1)}{(\pi \widehat{T}_\mathrm{w}(x_1)/\widehat{m}^\alpha)^{3/2}} \exp\left(-\frac{\widehat{m}^\alpha |\boldsymbol{\zeta}|^2}{\widehat{T}_\mathrm{w}(x_1)}\right). \tag{19}$$

The proof is a straightforward extension of that in Ref. [31] to gas mixtures and is omitted here. From Eq. (19), the coefficient functions $\hat{n}^\alpha_{(0)}$, $\hat{p}^\alpha_{(0)}$, etc. at $\mathrm{O}(\epsilon^0)$ are independent of x_2; in particular, the following relations hold:

$$\hat{\boldsymbol{v}}^\alpha_{(0)} = \hat{\boldsymbol{v}}_{(0)} = 0, \qquad \widehat{T}^\alpha_{(0)} = \widehat{T}_{(0)} = \widehat{T}_\mathrm{w}(x_1).$$

The first relation is due to the scaling discussed in the second paragraph of Section 2.3 (note that $\epsilon \sim \ell/L$). The second relation yields the following expressions for $\hat{p}^\alpha_{(0)}$ and $\hat{p}_{(0)}$:

$$\hat{p}^\alpha_{(0)} = \hat{n}^\alpha_{(0)} \widehat{T}_\mathrm{w}, \qquad \hat{p}_{(0)} = \hat{n}_{(0)} \widehat{T}_\mathrm{w}.$$

Remark 3. In the expression (19), $\hat{n}^\alpha_{(0)}$'s remain undetermined quantities. In Sections 2.4.2 and 2.4.3, we will proceed to the problem (17) at the first order and the problem (18) at the second order to derive the fluid-dynamic model describing their behaviour.

2.4.2. The solution $\hat{f}^\alpha_{(1)}$ of the problem (17)

The system (17) is a boundary-value problem for the inhomogeneous linear integro-differential equation for $\hat{f}^\alpha_{(1)}$. We introduce the new notation

$$y = \frac{x_2}{a}, \quad \phi^\alpha(s, x_1, y, \boldsymbol{c}) = \frac{\hat{f}^\alpha_{(1)}}{\hat{n}_{(0)} M(\boldsymbol{\zeta}; \widehat{m}^\alpha/\widehat{T}_\mathrm{w})}, \quad \boldsymbol{c} = \frac{\boldsymbol{\zeta}}{\sqrt{\widehat{T}_\mathrm{w}}},$$

and transform the system into that for ϕ^α. Taking into account Eq. (19), the relation $\chi^\alpha_{(0)} = \hat{n}^\alpha_{(0)}/\hat{n}_{(0)}$ and the energy conservation during molecular collisions ($\widehat{m}^\alpha|\boldsymbol{\zeta}|^2 + \widehat{m}^\beta|\boldsymbol{\zeta}_*|^2 = \widehat{m}^\alpha|\boldsymbol{\zeta}'|^2 + \widehat{m}^\beta|\boldsymbol{\zeta}'_*|^2$), we obtain the following boundary-value problem for the inhomogeneous linearized Boltzmann equation for ϕ^α:

$$c_2\partial_y\phi^\alpha = \frac{a\hat{n}_{(0)}}{\mathrm{K}_*}\sum_{\beta=\mathrm{A,B}} K^{\beta\alpha}L^{\beta\alpha}_{\widehat{T}_\mathrm{w}}\big(\chi^\alpha_{(0)}\phi^\beta, \chi^\beta_{(0)}\phi^\alpha\big) - a\chi^\alpha_{(0)}c_1\left[\frac{\partial_{x_1}\hat{p}_{(0)}}{\hat{p}_{(0)}} + \frac{\partial_{x_1}\chi^\alpha_{(0)}}{\chi^\alpha_{(0)}} + \left(\widehat{m}^\alpha|\boldsymbol{c}|^2 - \frac{5}{2}\right)\frac{\partial_{x_1}\widehat{T}_\mathrm{w}}{\widehat{T}_\mathrm{w}}\right], \tag{20a}$$

$$\phi^\alpha = \sigma_{2\pm}\big(\phi^\alpha(\boldsymbol{c})M\big(\boldsymbol{c};\widehat{m}^\alpha\big);\widehat{m}^\alpha\big), \quad c_2 \lessgtr 0,\ y = \pm\frac{1}{2}, \tag{20b}$$

where

$$L^{\beta\alpha}_\tau(f,g) = \int\big(f'_* + g' - f_* - g\big)M\big(\boldsymbol{c}_*;\widehat{m}^\beta\big)b^{\beta\alpha}_\tau\left(\frac{|\boldsymbol{e}\cdot\boldsymbol{C}|}{|\boldsymbol{C}|}, |\boldsymbol{C}|\right)\mathrm{d}\Omega(\boldsymbol{e})\,\mathrm{d}^3c_*, \tag{21a}$$

$$f'_* = f(\boldsymbol{c}'_*), \quad g' = g(\boldsymbol{c}'), \quad f_* = f(\boldsymbol{c}_*), \quad g = g(\boldsymbol{c}), \tag{21b}$$

$$\boldsymbol{c}' = \boldsymbol{c} + \frac{\hat{\mu}^{\beta\alpha}}{\widehat{m}^\alpha}(\boldsymbol{e}\cdot\boldsymbol{C})\boldsymbol{e}, \qquad \boldsymbol{c}'_* = \boldsymbol{c}_* - \frac{\hat{\mu}^{\beta\alpha}}{\widehat{m}^\beta}(\boldsymbol{e}\cdot\boldsymbol{C})\boldsymbol{e}, \tag{21c}$$

$$\boldsymbol{C} = \boldsymbol{c}_* - \boldsymbol{c}, \quad b^{\beta\alpha}_\tau\left(\frac{|\boldsymbol{e}\cdot\boldsymbol{C}|}{|\boldsymbol{C}|}, |\boldsymbol{C}|\right) = \frac{1}{\sqrt{\tau}}\,b^{\beta\alpha}\left(\frac{|\boldsymbol{e}\cdot\boldsymbol{C}|}{|\boldsymbol{C}|}, \sqrt{\tau}\,|\boldsymbol{C}|\right). \tag{21d}$$

It should be noted that here again s and x_1 occur as parameters in the problem. If we split the solution ϕ^α into even and odd parts with respect to c_1 as $\phi^\alpha = \phi^\alpha_\mathrm{even} + \phi^\alpha_\mathrm{odd}$, each part can be expressed as

$$\begin{aligned}
\phi^\alpha_\mathrm{even}(s,x_1,y,\boldsymbol{c}) &= \phi^\alpha_\mathrm{e}\big(y,\boldsymbol{c};\mathrm{K}(s,x_1,a),\chi^\mathrm{A}_{(0)}(s,x_1),\widehat{T}_\mathrm{w}(x_1)\big),\\
\phi^\alpha_\mathrm{odd}(s,x_1,y,\boldsymbol{c}) &= a\phi^\alpha_\mathrm{P}\big(y,\boldsymbol{c};\mathrm{K}(s,x_1,a),\chi^\mathrm{A}_{(0)}(s,x_1),\widehat{T}_\mathrm{w}(x_1)\big)\partial_{x_1}\ln\hat{p}_{(0)}\\
&\quad + a\phi^\alpha_\mathrm{T}(y,\boldsymbol{c};\mathrm{K}(s,x_1,a),\chi^\mathrm{A}_{(0)}(s,x_1),\widehat{T}_\mathrm{w}(x_1))\partial_{x_1}\ln\widehat{T}_\mathrm{w}\\
&\quad + a\phi^\alpha_\chi\big(y,\boldsymbol{c};\mathrm{K}(s,x_1,a),\chi^\mathrm{A}_{(0)}(s,x_1),\widehat{T}_\mathrm{w}(x_1)\big)\partial_{x_1}\chi^\mathrm{A}_{(0)},
\end{aligned}$$

where K is the local Knudsen number defined by

$$\mathrm{K}(s,x_1,a) = \frac{\mathrm{K}_*}{a\hat{n}_{(0)}(s,x_1)} = \frac{\mathrm{K}_*\widehat{T}_\mathrm{w}(x_1)}{a\hat{p}_{(0)}(s,x_1)},$$

and ϕ^α_e and ϕ^α_J ($J = \mathrm{P,T},\chi$) are the solutions of the following boundary-value problems:

$$c_2\partial_y\phi^\alpha_\mathrm{e} = \frac{1}{\mathrm{K}}\sum_{\beta=\mathrm{A,B}} K^{\beta\alpha}L^{\beta\alpha}_{\widehat{T}_\mathrm{w}}\big(\chi^\alpha_{(0)}\phi^\beta_\mathrm{e}, \chi^\beta_{(0)}\phi^\alpha_\mathrm{e}\big), \tag{22a}$$

$$\phi^\alpha_\mathrm{e} = \sigma_{2\pm}\big(\phi^\alpha_\mathrm{e}(\boldsymbol{c})M\big(\boldsymbol{c};\widehat{m}^\alpha\big);\widehat{m}^\alpha\big), \quad c_2 \lessgtr 0,\ y = \pm\frac{1}{2}, \tag{22b}$$

and

$$c_2\partial_y\phi^\alpha_J = \frac{1}{\mathrm{K}}\sum_{\beta=\mathrm{A,B}} K^{\beta\alpha}L^{\beta\alpha}_{\widehat{T}_\mathrm{w}}\big(\chi^\alpha_{(0)}\phi^\beta_J, \chi^\beta_{(0)}\phi^\alpha_J\big) - I^\alpha_J, \tag{23a}$$

$$\phi^\alpha_J = 0, \quad c_2 \lessgtr 0,\ y = \pm\frac{1}{2}, \tag{23b}$$

with I^α_J being the following:

$$I^\alpha_\mathrm{P} = c_1\chi^\alpha_{(0)}, \quad I^\mathrm{A}_\chi = c_1, \quad I^\mathrm{B}_\chi = -c_1, \quad I^\alpha_\mathrm{T} = \chi^\alpha_{(0)}c_1\left(\widehat{m}^\alpha|\boldsymbol{c}|^2 - \frac{5}{2}\right).$$

The solution ϕ^α_e of the problem (22) can be shown to be independent of both y and c_i

$$\phi^\alpha_\mathrm{e} = \phi^\alpha_\mathrm{e}(s,x_1).$$

The proof is omitted here for conciseness. (The proof relies on the *non-positivity* of the linearized collision operator; see Ref. [32] and Appendix A.12 in Ref. [29].) On the other hand, ϕ^α_P, ϕ^α_T and ϕ^α_χ are, respectively, the solutions for the

three elemental flow problems: the flow caused by the pressure gradient (Poiseuille flow), the flow by the temperature gradient (thermal transpiration) and the flow by the concentration gradient. (See, for instance, Ref. [22].)

To summarize, $\hat{f}^{\alpha}_{(1)}$ can be expressed in terms of the solutions of elemental problems $\phi^{\alpha}_{\rm e}$, $\phi^{\alpha}_{\rm P}$, $\phi^{\alpha}_{\rm T}$ and ϕ^{α}_{χ}, as

$$\begin{aligned}\hat{f}^{\alpha}_{(1)} &= \hat{n}_{(0)} M\left(\boldsymbol{\zeta}; \frac{\widehat{m}^{\alpha}}{\widehat{T}_{\rm w}}\right)\left(\phi^{\alpha}_{\rm e}\left(x_2/a, \boldsymbol{\zeta}/\sqrt{\widehat{T}_{\rm w}}; {\rm K}(s, x_1, a), \chi^{\rm A}_{(0)}(s, x_1), \widehat{T}_{\rm w}(x_1)\right)\right.\\ &\quad + a\phi^{\alpha}_{\rm P}\left(x_2/a, \boldsymbol{\zeta}/\sqrt{\widehat{T}_{\rm w}}; {\rm K}(s, x_1, a), \chi^{\rm A}_{(0)}(s, x_1), \widehat{T}_{\rm w}(x_1)\right)\partial_{x_1}\ln\hat{p}_{(0)}\\ &\quad + a\phi^{\alpha}_{\rm T}\left(x_2/a, \boldsymbol{\zeta}/\sqrt{\widehat{T}_{\rm w}}; {\rm K}(s, x_1, a), \chi^{\rm A}_{(0)}(s, x_1), \widehat{T}_{\rm w}(x_1)\right)\partial_{x_1}\ln\widehat{T}_{\rm w}\\ &\quad + a\phi^{\alpha}_{\chi}\left(x_2/a, \boldsymbol{\zeta}/\sqrt{\widehat{T}_{\rm w}}; {\rm K}(s, x_1, a), \chi^{\rm A}_{(0)}(s, x_1), \widehat{T}_{\rm w}(x_1)\right)\left.\partial_{x_1}\chi^{\rm A}_{(0)}\right). \end{aligned} \tag{24}$$

From this result, the following expressions of the coefficient functions of the macroscopic quantities at the first order of ϵ are obtained:

$$\hat{n}^{\alpha}_{(1)} = \hat{n}_{(0)}\int \phi^{\alpha}_{\rm e} M\left(\boldsymbol{c}; \widehat{m}^{\alpha}\right){\rm d}^3 c = \hat{n}_{(0)}\phi^{\alpha}_{\rm e}, \tag{25}$$

$$\hat{n}^{\alpha}_{(0)}\hat{v}^{\alpha}_{1(1)} = a\,\hat{n}_{(0)}\sqrt{\widehat{T}_{\rm w}}\left(u^{\alpha}_{\rm P}\partial_{x_1}\ln\hat{p}_{(0)} + u^{\alpha}_{\rm T}\partial_{x_1}\ln\widehat{T}_{\rm w} + u^{\alpha}_{\chi}\partial_{x_1}\chi^{\rm A}_{(0)}\right), \tag{26}$$

$$u^{\alpha}_{J} = \int c_1\phi^{\alpha}_{J}(\boldsymbol{c}) M\left(\boldsymbol{c}; \widehat{m}^{\alpha}\right){\rm d}^3 c \quad (J = {\rm P}, {\rm T}, \chi), \tag{27}$$

$$\hat{v}^{\alpha}_{2(1)} = \hat{v}^{\alpha}_{3(1)} = \widehat{T}^{\alpha}_{(1)} = 0. \tag{28}$$

2.4.3. The problem (18) and the fluid-dynamic model

The system (18) is a boundary-value problem for the inhomogeneous linear integro-differential equation for $\hat{f}^{\alpha}_{(2)}$. Here we are not going to solve this problem. Instead, by considering the particle conservation of each species, we shall derive a set of fluid-dynamic equations describing the behaviour of $\hat{n}^{\alpha}_{(0)}$'s. The resulting set of equations provides a one-dimensional fluid-dynamic model for the gas mixture in the channel.

We first integrate Eq. (18a) with respect to $\boldsymbol{\zeta}$ in its whole space and with respect to x_2 from $-a/2$ to $a/2$ to have

$$a\partial_s\hat{n}^{\alpha}_{(0)} + \partial_{x_1}\int_{-a/2}^{a/2}\hat{n}^{\alpha}_{(0)}\hat{v}^{\alpha}_{1(1)}\,{\rm d}x_2 + \left[\int \zeta_2\hat{f}^{\alpha}_{(2)}\,{\rm d}^3\zeta\right]_{x_2=-a/2}^{x_2=a/2} = 0,$$

where the facts that the contribution of collision terms vanishes in the first integration because of their basic property and that $\hat{n}^{\alpha}_{(0)}$ is independent of x_2 have been taken into account. This relation represents the particle conservation for species α in the channel. It should be noted that the last term on the left-hand side vanishes because of the boundary condition (18b). Substituting Eq. (26) into the second term and using the relation between y and x_2, we arrive at

$$\begin{aligned}&\partial_s\hat{n}^{\alpha}_{(0)} + \partial_{x_1}\mathcal{J}^{\alpha} = 0,\\ &\mathcal{J}^{\alpha} = a\left(\mathcal{M}^{\alpha}_{\rm P}\partial_{x_1}\ln\hat{p}_{(0)} + \mathcal{M}^{\alpha}_{\rm T}\partial_{x_1}\ln\widehat{T}_{\rm w} + \mathcal{M}^{\alpha}_{\chi}\partial_{x_1}\chi^{\rm A}_{(0)}\right)\frac{\hat{p}_{(0)}}{\sqrt{\widehat{T}_{\rm w}}},\end{aligned}$$

where

$$\mathcal{M}^{\alpha}_{J}\left({\rm K}, \chi^{\rm A}_{(0)}, \widehat{T}_{\rm w}\right) = \int_{-1/2}^{1/2} u^{\alpha}_{J}\,{\rm d}y \quad (J = {\rm P}, {\rm T}, \chi).$$

The physical meaning of $\mathcal{J}^{\alpha}$ is the particle flux N^{α}_{f} of species α through the channel nondimensionalized by the factor of $n_* D\epsilon\,(2kT_*/m^{\rm A})^{1/2}$. Since $\hat{p}_{(0)}$ (or $\hat{n}_{(0)}$) and $\chi^{\rm A}_{(0)}$ can be expressed in terms of $\hat{n}^{\alpha}_{(0)}$'s, this is a closed set of equations for $\hat{n}^{\rm A}_{(0)}$ and $\hat{n}^{\rm B}_{(0)}$. After some manipulations, we finally obtain the following closed set of equations for $\hat{p}_{(0)}$ and $\chi^{\rm A}_{(0)}$:

$$\partial_s \hat{p}_{(0)} \chi^{\mathrm{A}}_{(0)} + \widehat{T}_{\mathrm{w}} \partial_{x_1} \mathcal{J}^{\mathrm{A}} = 0, \tag{29a}$$

$$\partial_s \hat{p}_{(0)} + \widehat{T}_{\mathrm{w}} \partial_{x_1} \mathcal{J} = 0, \tag{29b}$$

where

$$\mathcal{J} = \mathcal{J}^{\mathrm{A}} + \mathcal{J}^{\mathrm{B}} = a\big(\mathcal{M}_{\mathrm{P}} \partial_{x_1} \ln \hat{p}_{(0)} + \mathcal{M}_{\mathrm{T}} \partial_{x_1} \ln \widehat{T}_{\mathrm{w}} + \mathcal{M}_{\chi} \partial_{x_1} \chi^{\mathrm{A}}_{(0)}\big) \frac{\hat{p}_{(0)}}{\sqrt{\widehat{T}_{\mathrm{w}}}},$$

$$\mathcal{M}_J = \mathcal{M}^{\mathrm{A}}_J + \mathcal{M}^{\mathrm{B}}_J \quad (J = \mathrm{P}, \mathrm{T}, \chi).$$

Eq. (29) is a set of convection–diffusion-type fluid-dynamic equations with $\mathcal{M}_{\mathrm{P}}$, $\mathcal{M}_{\mathrm{T}}$, etc. being the *diffusion coefficients* and with the convection due to the gradient of temperature. We call this set the (one-dimensional) fluid-dynamic model in the straight two-dimensional channel.

Remark 4. In order to obtain the diffusion coefficients $\mathcal{M}_{\mathrm{P}}$, $\mathcal{M}_{\mathrm{T}}$, etc. explicitly to complete Eq. (29), the analyses of the linearized problem (23) for the three elemental flows are necessary. Since the problems cannot be solved analytically, one has to construct a numerical database that yields, instantaneously, the values of those coefficients for arbitrary values of the parameters K, $\chi^{\mathrm{A}}_{(0)}$ and $\widehat{T}_{\mathrm{w}}$. In the present work, such a database is constructed by the use of model Boltzmann equations (see Appendix A).

Remark 5. The diffusion coefficients $\mathcal{M}_{\mathrm{P}}$, $\mathcal{M}_{\mathrm{T}}$, etc. diverge with the rate of $\ln \mathrm{K}$ as $\mathrm{K} \to \infty$ [33–35]. This corresponds to the fact that, in the free-molecular limit, the appropriate time scale is not t_* in Section 2.3 but rather $t_*/\ln(L/D_*)$. This is mathematically shown in Refs. [36] and [37] in the case of single-species gases. Incidentally, in the case of the flows in a pipe, the appropriate time scale is always t_* with D_* being the internal (or external) diameter, irrespective of the value of K. Mathematical discussions on the description of diffusion process in the free-molecular limit was started for this case in Refs. [38] and [39].

3. Junction of the channels of different uniform widths

In this section, we shall consider the gas mixture in the channel composed of two elemental channels of different uniform widths. The flow in the channel is no longer unidirectional. However, as far as the widths of channels are small enough compared to the characteristic length of variation of the wall temperature, the influence of the junction is expected to be limited near there, because the Reynolds number is of O(1), and the overall behaviour of the mixture in each elemental channel can be described by the fluid-dynamic model derived in Section 2. We shall derive the connection condition at the junction for this model.

For simplicity, we shall first discuss, in Section 3.1, the problem in the case where the elemental channels are connected with sharing the centre line and derive the connection condition for this simplest case. Then, in Section 3.2, we briefly describe the extension of the result to more general cases.

3.1. Junction problem for two elemental channels sharing the centre line

Consider a binary gas mixture in the channel composed of two elemental channels, say element I and element II, of different uniform widths connected at $X_1 = 0$ with sharing the centre line (Fig. 3). The width D_{I} of element I is

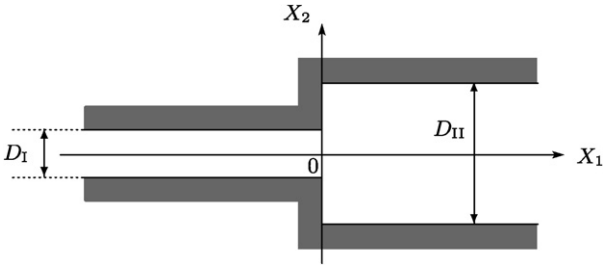

Fig. 3. Schematic of the junction of two elemental channels sharing the centre line.

smaller than that of element II, $D_{\rm II}$. The temperature $T_{\rm w}$ of the channel walls is kept constant in time and depends only on X_1, i.e., $T_{\rm w}(X_1)$. At the junction ($X_1 = 0$), the temperature $T_{\rm w}$ is continuous, but its gradient may be discontinuous in general. We assume that in each element the behaviour of the gas mixture can be described by the Boltzmann equation and the velocity distribution function is continuous at the junction. We also assume the diffuse reflection boundary condition on the walls.

By the use of the same reference quantities as in Section 2.3, we have the dimensionless description of the problem in the following form: for $x_1 \lessgtr 0$

$$\epsilon^2 \partial_s F^\alpha + \epsilon \zeta_1 \partial_{x_1} F^\alpha + \zeta_2 \partial_{x_2} F^\alpha = \frac{1}{\mathrm{K}_*} \sum_{\beta=\mathrm{A,B}} K^{\beta\alpha} \hat{J}^{\beta\alpha}\big(F^\beta, F^\alpha\big), \tag{30a}$$

$$F^\alpha = \sigma_{2\pm}\left(F^\alpha(\boldsymbol{\zeta}); \frac{\widehat{m}^\alpha}{\widehat{T}_{\rm w}}\right) M\left(\boldsymbol{\zeta}; \frac{\widehat{m}^\alpha}{\widehat{T}_{\rm w}}\right), \quad \zeta_2 \lessgtr 0,\ x_2 = \pm\frac{a_J}{2}, \tag{30b}$$

and at the junction ($x_1 = 0$)

$$F^\alpha = \sigma_{1-}\left(F^\alpha(\boldsymbol{\zeta}); \frac{\widehat{m}^\alpha}{\widehat{T}_{\rm w}}\right) M\left(\boldsymbol{\zeta}; \frac{\widehat{m}^\alpha}{\widehat{T}_{\rm w}}\right), \quad \zeta_1 > 0,\ \frac{a_{\rm I}}{2} < |x_2| < \frac{a_{\rm II}}{2}, \tag{31a}$$

$$F^\alpha(s, x_1 = 0_-, x_2, \boldsymbol{\zeta}) = F^\alpha(s, x_1 = 0_+, x_2, \boldsymbol{\zeta}), \quad |x_2| < \frac{a_{\rm I}}{2}, \tag{31b}$$

where $J = \mathrm{I}$ for $x_1 < 0$ and $J = \mathrm{II}$ for $x_1 > 0$ in Eq. (30b) and

$$a_{\rm I} = D_{\rm I}/D_*, \qquad a_{\rm II} = D_{\rm II}/D_*.$$

Here, we denote the dimensionless distribution function by F^α in order to avoid the confusion with the solution $\hat{f}^\alpha$ of the problem in Section 2.

As is readily seen, $\hat{f}^\alpha_{(0)}$ solves the problem (30) and (31) with ϵ being zero if $\hat{n}^\alpha_{(0)}(s, x_1 = 0_-) = \hat{n}^\alpha_{(0)}(s, x_1 = 0_+)$, or equivalently

$$\hat{p}_{(0)}(s, x_1 = 0_-) = \hat{p}_{(0)}(s, x_1 = 0_+), \tag{32a}$$

$$\chi^{\rm A}_{(0)}(s, x_1 = 0_-) = \chi^{\rm A}_{(0)}(s, x_1 = 0_+). \tag{32b}$$

That is, as far as the order of ϵ^0 is concerned, one can construct the solution of the present problem by the solution of the problem in Section 2 with the continuity condition (32). However, if one proceeds to the order of ϵ, the same is not true because $\hat{f}^\alpha_{(1)}$ does not satisfy the diffuse reflection condition at the junction [see Eq. (31a)]. We have to introduce the correction g^α to $\hat{f}^\alpha$ and represent the solution F^α in the form

$$F^\alpha = \hat{f}^\alpha + g^\alpha. \tag{33}$$

Here the correction function g^α is supposed to change rapidly in x_1, i.e., $\partial_{x_1} g^\alpha = \mathrm{O}(g^\alpha)/\epsilon$, and to be appreciable only in the vicinity of the junction. As in Section 2.4, we expand g^α in a power series of ϵ. Since $\hat{f}^\alpha_{(0)}$ solves the problem at the zero-th order, this expansion starts from the first order:

$$g^\alpha = g^\alpha_{(1)}\epsilon + g^\alpha_{(2)}\epsilon^2 + \cdots.$$

Substituting Eq. (33) with the expansions of $\hat{f}^\alpha$ and g^α into Eqs. (30) and (31) and equating like powers of ϵ lead to a series of boundary-value problems for $g^\alpha_{(1)}$, $g^\alpha_{(2)}$, ... With the stretched coordinate z defined by $z = x_1/\epsilon$, the boundary-value problem for $g^\alpha_{(1)}$ can be described as follows: for $z \lessgtr 0$

$$\zeta_1 \partial_z g^\alpha_{(1)} + \zeta_2 \partial_{x_2} g^\alpha_{(1)} = \frac{1}{\mathrm{K}_*} \sum_{\beta=\mathrm{A,B}} K^{\beta\alpha}\big[\hat{J}^{\beta\alpha}\big(\hat{f}^\beta_{(0)\pm}, g^\alpha_{(1)}\big) + \hat{J}^{\beta\alpha}\big(g^\beta_{(1)}, \hat{f}^\alpha_{(0)\pm}\big)\big], \tag{34a}$$

$$g^\alpha_{(1)} = \sigma_{2\pm}\left(g^\alpha_{(1)}(\boldsymbol{\zeta}); \frac{\widehat{m}^\alpha}{\widehat{T}_{\rm w}(0)}\right) M\left(\boldsymbol{\zeta}; \frac{\widehat{m}^\alpha}{\widehat{T}_{\rm w}(0)}\right), \quad \zeta_2 \lessgtr 0,\ x_2 = \pm\frac{a_J}{2}, \tag{34b}$$

at the junction ($z = 0$)

$$g^{\alpha}_{(1)} = \sigma_{1-}\left(g^{\alpha}_{(1)}(\boldsymbol{\zeta}) + \hat{f}^{\alpha}_{(1)+}(\boldsymbol{\zeta}); \frac{\widehat{m}^{\alpha}}{\widehat{T}_{\mathrm{w}}}\right) M\left(\boldsymbol{\zeta}; \frac{\widehat{m}^{\alpha}}{\widehat{T}_{\mathrm{w}}}\right) - \hat{f}^{\alpha}_{(1)+}, \quad \zeta_1 > 0, \ \frac{a_{\mathrm{I}}}{2} < |x_2| < \frac{a_{\mathrm{II}}}{2}, \tag{35a}$$

$$g^{\alpha}_{(1)}(s, z = 0_-, x_2, \boldsymbol{\zeta}) + \hat{f}^{\alpha}_{(1)-} = g^{\alpha}_{(1)}(s, z = 0_+, x_2, \boldsymbol{\zeta}) + \hat{f}^{\alpha}_{(1)+}, \quad |x_2| < \frac{a_{\mathrm{I}}}{2}, \tag{35b}$$

and at a far distance from the junction ($|z| \to \infty$)

$$g^{\alpha}_{(1)} \to 0, \tag{36}$$

where $J = \mathrm{I}$ for $z < 0$ and $J = \mathrm{II}$ for $z > 0$ in Eq. (34b) and $\hat{f}^{\alpha}_{(0)\pm}$ and $\hat{f}^{\alpha}_{(1)\pm}$ represent their values at $x_1 = 0_{\pm}$. In Eq. (34a), $\hat{f}^{\alpha}_{(0)+}$ is for $z > 0$ and $\hat{f}^{\alpha}_{(0)-}$ for $z < 0$. It should be noted that in Eq. (34b), as well as in Eq. (35a), $\widehat{T}_{\mathrm{w}}$ denotes the dimensionless temperature at the junction ($x_1 = 0$). In the rest of the paper, we admit the existence of the solution of the problem (34)–(36) and simply examine the necessary condition for the solution to exist. As will be clear from the derivation below, the necessary condition is essentially the particle conservation; and it provides, together with the continuity condition (32), the connection condition at the junction for the fluid-dynamic model.

We start with integrating Eq. (34) with respect to $\boldsymbol{\zeta}$ in its whole space and with respect to x_2 from $-a_{\mathrm{I}}/2$ to $a_{\mathrm{I}}/2$ for $z < 0$ and from $-a_{\mathrm{II}}/2$ to $a_{\mathrm{II}}/2$ for $z > 0$ to have

$$\partial_z \int_{-a_{\mathrm{I}}/2}^{a_{\mathrm{I}}/2} \int \zeta_1 g^{\alpha}_{(1)} \, \mathrm{d}^3\zeta \, \mathrm{d}x_2 = 0, \quad z < 0,$$

$$\partial_z \int_{-a_{\mathrm{II}}/2}^{a_{\mathrm{II}}/2} \int \zeta_1 g^{\alpha}_{(1)} \, \mathrm{d}^3\zeta \, \mathrm{d}x_2 = 0, \quad z > 0.$$

Here the property of the collision terms and the diffuse reflection condition (34b) have been taken into account in the first and second integrations, respectively. The resulting equations, with the aid of the condition (36), lead to

$$\int_{-a_{\mathrm{I}}/2}^{a_{\mathrm{I}}/2} \int \zeta_1 g^{\alpha}_{(1)}(s, z = 0_-, x_2, \boldsymbol{\zeta}) \, \mathrm{d}^3\zeta \, \mathrm{d}x_2 = 0, \tag{37a}$$

$$\int_{-a_{\mathrm{II}}/2}^{a_{\mathrm{II}}/2} \int \zeta_1 g^{\alpha}_{(1)}(s, z = 0_+, x_2, \boldsymbol{\zeta}) \, \mathrm{d}^3\zeta \, \mathrm{d}x_2 = 0. \tag{37b}$$

In the meantime, from condition (35), $g^{\alpha}_{(1)}$ must satisfy

$$\int_{a_{\mathrm{I}}/2 < |x_2| < a_{\mathrm{II}}/2} \int \zeta_1 \left[g^{\alpha}_{(1)}(s, z = 0_+, x_2, \boldsymbol{\zeta}) + \hat{f}^{\alpha}_{(1)+}\right] \mathrm{d}^3\zeta \, \mathrm{d}x_2 = 0, \tag{38}$$

and

$$\int_{-a_{\mathrm{I}}/2}^{a_{\mathrm{I}}/2} \int \zeta_1 \left[g^{\alpha}_{(1)}(s, z = 0_-, x_2, \boldsymbol{\zeta}) + \hat{f}^{\alpha}_{(1)-}\right] \mathrm{d}^3\zeta \, \mathrm{d}x_2 = \int_{-a_{\mathrm{I}}/2}^{a_{\mathrm{I}}/2} \int \zeta_1 \left[g^{\alpha}_{(1)}(s, z = 0_+, x_2, \boldsymbol{\zeta}) + \hat{f}^{\alpha}_{(1)+}\right] \mathrm{d}^3\zeta \, \mathrm{d}x_2. \tag{39}$$

Combining the conditions (37)–(39) all together, we have

$$\int_{-a_{\mathrm{I}}/2}^{a_{\mathrm{I}}/2} \int \zeta_1 \hat{f}^{\alpha}_{(1)-} \, \mathrm{d}^3\zeta \, \mathrm{d}x_2 = \int_{-a_{\mathrm{II}}/2}^{a_{\mathrm{II}}/2} \int \zeta_1 \hat{f}^{\alpha}_{(1)+} \, \mathrm{d}^3\zeta \, \mathrm{d}x_2,$$

which is finally reduced to

$$a_{\mathrm{I}} \mathcal{J}^{\mathrm{A}}(s, x_1 = 0_-) = a_{\mathrm{II}} \mathcal{J}^{\mathrm{A}}(s, x_1 = 0_+), \tag{40a}$$

$$a_{\mathrm{I}} \mathcal{J}(s, x_1 = 0_-) = a_{\mathrm{II}} \mathcal{J}(s, x_1 = 0_+). \tag{40b}$$

The set of Eqs. (32) and (40) is the connection condition for the fluid-dynamic model (29) at the junction.

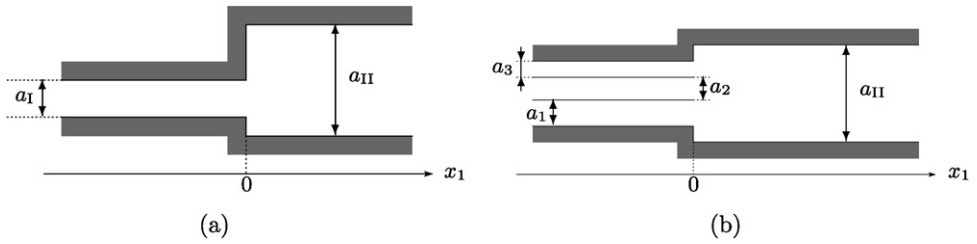

Fig. 4. Schematic of junctions in general cases. (a) Junction of two elemental channels. (b) Junction of multiple narrow channels and one wide channel in the case of $N = 3$. Dimensionless notation is used in the figure.

3.2. Connection condition for more general cases

In Section 3.1, we have derived the connection condition at the junction in the case where two elemental channels share the centre line. We shall first remove this restriction and consider the connection condition at the junction of two elemental channels not necessarily sharing the centre line, as depicted in Fig. 4(a). This extension can be readily done, in a way parallel to the analysis in Section 3.1, to conclude that the connection condition, Eqs. (32) and (40), remains unchanged. This is due to the fact that $\hat{n}^{\alpha}_{(0)}$ does not depend on x_2 and that Eq. (40) comes from the property of the quantity integrated with respect to x_2 over each elemental channel.

Next we consider the case where N elemental narrow channels are connected to one elemental thick channel at $x_1 = 0$, as depicted in Fig. 4(b). We number the elements in $x_1 < 0$ from 1 to N and denote the dimensionless width of the i-th element by a_i $(i = 1, \ldots, N)$, while we call the element in $x_1 > 0$ the element II and denote its dimensionless width by $a_{\rm II}$. The independence of the connection condition on the position in x_2 in the previous paragraph provides a clear perspective for the extension to this case. In fact, assuming $a_1 + \cdots + a_N \leqslant a_{\rm II}$, the extension of the discussion in Section 3.1 yields the following connection condition, which is a natural and simple extension of Eqs. (32) and (40):

$$\hat{p}_{(0)}(s, x_1 = 0_-; i) = \hat{p}_{(0)}(s, x_1 = 0_+), \quad i = 1, \ldots, N, \tag{41a}$$

$$\chi^{\rm A}_{(0)}(s, x_1 = 0_-; i) = \chi^{\rm A}_{(0)}(s, x_1 = 0_+), \quad i = 1, \ldots, N, \tag{41b}$$

and

$$\sum_{i=1}^{N} a_i \mathcal{J}^{\rm A}(s, x_1 = 0_-; i) = a_{\rm II}\mathcal{J}^{\rm A}(s, x_1 = 0_+), \tag{42a}$$

$$\sum_{i=1}^{N} a_i \mathcal{J}(s, x_1 = 0_-; i) = a_{\rm II}\mathcal{J}(s, x_1 = 0_+). \tag{42b}$$

Here the argument i of the quantities in Eqs. (41) and (42) indicates that the quantity is evaluated in the i-th elemental channel. The set of Eqs. (41) and (42) is the connection condition for the second extension.

4. Fluid-dynamic model for the Knudsen compressor

With the results of the analyses in Sections 2 and 3, we are ready to present the fluid-dynamic model for the behaviour of the gas mixture in the Knudsen compressor.

Consider the Knudsen compressor composed of $\mathcal{N}$ elemental units of length L arranged in the X_1-direction as depicted in Fig. 5. The elemental unit is composed of two subunits, subunit I of length $L_{\rm I}$ and width $D_{\rm I}$ and subunit II of length $L_{\rm II}$ and width $D_{\rm II}$, where $L = L_{\rm I} + L_{\rm II}$ and $D_{\rm I} \leqslant D_{\rm II}$. The subunit II is a channel of uniform width $D_{\rm II}$, while the subunit I is composed of N elemental channels numbered from 1 to N. We denote the width of the i-th elemental channel by D_i $(D_{\rm I} = D_1 + \cdots + D_N)$. The temperature $T_{\rm w}$ of the wall, including the shelves separating each subunit I into N channels, is constant in time and depends only on X_1. (In particular, the distribution of wall temperature in subunit I is common to N elemental channels.) The temperature $T_{\rm w}(X_1)$ varies smoothly in each subunit, is continuous at junctions and is periodic with period L, i.e., $T_{\rm w}(X_1) = T_{\rm w}(X_1 + L)$ $[0 \leqslant X_1 \leqslant (\mathcal{N} - 1)L]$.

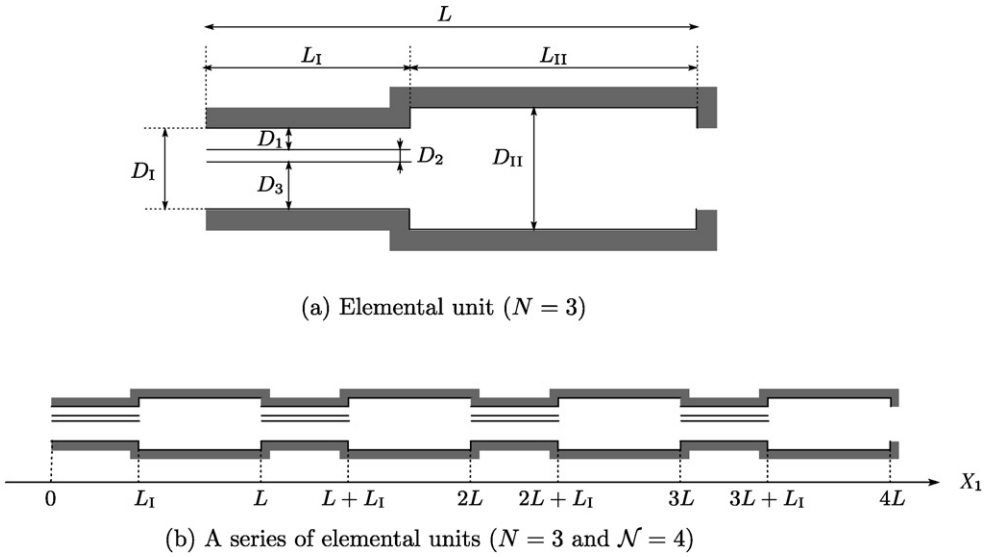

Fig. 5. Schematic of the Knudsen compressor.

If individual elemental channels, channels i ($i = 1, \dots, N$) and II, are long enough, i.e., $D_i/L_{\rm I} \ll 1$ and $D_{\rm II}/L_{\rm II} \ll 1$, and their widths D_i and $D_{\rm II}$ are comparable to the mean free path of gas molecules, we can make use of the results in Sections 2 and 3 for the description of the gas behaviour in the device. That is, the behaviour of the gas mixture in the Knudsen compressor can be described by the fluid-dynamic model (29) for the individual elemental channels with the connection conditions (41) and (42). Here, with the new notation

$$r_{\rm I} = L_{\rm I}/L, \qquad r_{\rm II} = L_{\rm II}/L \ (= 1 - r_{\rm I}),$$

we present the (dimensionless) fluid-dynamic model for the gas mixture in the Knudsen compressor:

In the i-th element of subunit I: for $j < x_1 < j + r_{\rm I}$ ($j = 0, 1, \dots, \mathcal{N} - 1$)

$$\partial_s \hat{p}_i \chi_i^{\rm A} + \widehat{T}_{\rm w} \partial_{x_1} \mathcal{J}_i^{\rm A} = 0, \tag{43a}$$

$$\mathcal{J}_i^{\rm A} = a_i \big(\mathcal{M}_{\rm P}^{\rm A}(\mathrm{K}_i, \chi_i^{\rm A}, \widehat{T}_{\rm w}) \partial_{x_1} \ln \hat{p}_i + \mathcal{M}_{\rm T}^{\rm A}(\mathrm{K}_i, \chi_i^{\rm A}, \widehat{T}_{\rm w}) \partial_{x_1} \ln \widehat{T}_{\rm w} + \mathcal{M}_{\chi}^{\rm A}(\mathrm{K}_i, \chi_i^{\rm A}, \widehat{T}_{\rm w}) \partial_{x_1} \chi_i^{\rm A} \big) \frac{\hat{p}_i}{\sqrt{\widehat{T}_{\rm w}}}, \tag{43b}$$

$$\partial_s \hat{p}_i + \widehat{T}_{\rm w} \partial_{x_1} \mathcal{J}_i = 0, \tag{44a}$$

$$\mathcal{J}_i = a_i \big(\mathcal{M}_{\rm P}(\mathrm{K}_i, \chi_i^{\rm A}, \widehat{T}_{\rm w}) \partial_{x_1} \ln \hat{p}_i + \mathcal{M}_{\rm T}(\mathrm{K}_i, \chi_i^{\rm A}, \widehat{T}_{\rm w}) \partial_{x_1} \ln \widehat{T}_{\rm w} + \mathcal{M}_{\chi}(\mathrm{K}_i, \chi_i^{\rm A}, \widehat{T}_{\rm w}) \partial_{x_1} \chi_i^{\rm A} \big) \frac{\hat{p}_i}{\sqrt{\widehat{T}_{\rm w}}}. \tag{44b}$$

In the subunit II: for $j + r_{\rm I} < x_1 < j + 1$ ($j = 0, 1, \dots, \mathcal{N} - 1$)

$$\partial_s \hat{p}_{\rm II} \chi_{\rm II}^{\rm A} + \widehat{T}_{\rm w} \partial_{x_1} \mathcal{J}_{\rm II}^{\rm A} = 0, \tag{45a}$$

$$\mathcal{J}_{\rm II}^{\rm A} = a_{\rm II} \big(\mathcal{M}_{\rm P}^{\rm A}(\mathrm{K}_{\rm II}, \chi_{\rm II}^{\rm A}, \widehat{T}_{\rm w}) \partial_{x_1} \ln \hat{p}_{\rm II} + \mathcal{M}_{\rm T}^{\rm A}(\mathrm{K}_{\rm II}, \chi_{\rm II}^{\rm A}, \widehat{T}_{\rm w}) \partial_{x_1} \ln \widehat{T}_{\rm w} + \mathcal{M}_{\chi}^{\rm A}(\mathrm{K}_{\rm II}, \chi_{\rm II}^{\rm A}, \widehat{T}_{\rm w}) \partial_{x_1} \chi_{\rm II}^{\rm A} \big) \frac{\hat{p}_{\rm II}}{\sqrt{\widehat{T}_{\rm w}}}, \tag{45b}$$

$$\partial_s \hat{p}_{\rm II} + \widehat{T}_{\rm w} \partial_{x_1} \mathcal{J}_{\rm II} = 0, \tag{46a}$$

$$\mathcal{J}_{\rm II} = a_{\rm II} \big(\mathcal{M}_{\rm P}(\mathrm{K}_{\rm II}, \chi_{\rm II}^{\rm A}, \widehat{T}_{\rm w}) \partial_{x_1} \ln \hat{p}_{\rm II} + \mathcal{M}_{\rm T}(\mathrm{K}_{\rm II}, \chi_{\rm II}^{\rm A}, \widehat{T}_{\rm w}) \partial_{x_1} \ln \widehat{T}_{\rm w} + \mathcal{M}_{\chi}(\mathrm{K}_{\rm II}, \chi_{\rm II}^{\rm A}, \widehat{T}_{\rm w}) \partial_{x_1} \chi_{\rm II}^{\rm A} \big) \frac{\hat{p}_{\rm II}}{\sqrt{\widehat{T}_{\rm w}}}. \tag{46b}$$

At junctions: at $x_1 = r_{\rm I}, j, r_{\rm I} + j$ ($j = 1, \dots, \mathcal{N} - 1$)

$$\chi_i^{\rm A} = \chi_{\rm II}^{\rm A}, \qquad \hat{p}_i = \hat{p}_{\rm II}, \tag{47a}$$

$$\sum_{i=1}^{N} a_i \mathcal{J}_i^{\rm A} = a_{\rm II} \mathcal{J}_{\rm II}^{\rm A}, \qquad \sum_{i=1}^{N} a_i \mathcal{J}_i = a_{\rm II} \mathcal{J}_{\rm II}, \tag{47b}$$

where $\hat{p}_i$ and χ_i^{A} denote $\hat{p}_{(0)}$ and $\chi_{(0)}^{\mathrm{A}}$ in the i-th elemental channel in subunit I, $\hat{p}_{\mathrm{II}}$ and $\chi_{\mathrm{II}}^{\mathrm{A}}$ those in the subunit II and K_i and K_{II} the local Knudsen numbers in the i-th elemental channel and in the subunit II defined by

$$\mathrm{K}_i = \frac{\widehat{T}_{\mathrm{w}}}{a_i \hat{p}_i}\mathrm{K}_*, \qquad \mathrm{K}_{\mathrm{II}} = \frac{\widehat{T}_{\mathrm{w}}}{a_{\mathrm{II}} \hat{p}_{\mathrm{II}}}\mathrm{K}_*.$$

The quantities $\mathcal{J}_i^{\mathrm{A}}$ and $\mathcal{J}_i$ denote the dimensionless particle fluxes of species A and of the mixture through the i-th elemental channel nondimensionalized by $n_* D_i \epsilon (2kT_*/m^{\mathrm{A}})^{1/2}$; $\mathcal{J}_{\mathrm{II}}^{\mathrm{A}}$ and $\mathcal{J}_{\mathrm{II}}$ the counterparts through the subunit II nondimensionalized by $n_* D_{\mathrm{II}} \epsilon (2kT_*/m^{\mathrm{A}})^{1/2}$.

With initial conditions for χ_i^{A}, $\chi_{\mathrm{II}}^{\mathrm{A}}$, $\hat{p}_i$ and $\hat{p}_{\mathrm{II}}$ and with proper boundary conditions at the both ends of the compressor (at $x_1 = 0$ and $\mathcal{N}$), we can describe the time evolution of the pressure and concentration distributions in the device by the fluid-dynamic model (43)–(47). In the numerical simulations in the subsequent section, we shall use the following boundary conditions at the ends of the compressor, depending on whether the end is open or closed, which would be simplest and natural:

(i) Open end (or the end connected to a reservoir huge enough): the concentration of species A and the pressure of the mixture are given.
(ii) Closed end: there are no particle fluxes of species A and of the mixture.

Before closing this section, it should be noted that the fluid-dynamic model summarized above describes the behaviour of the mixture in the limit of the infinitesimal aspect ratio of elemental channels: $\epsilon = 0_+$ or $D_{\mathrm{I}}/L = 0_+$.

5. Numerical results and discussions

5.1. Preliminary test of the fluid-dynamic model

In order to assess the practical reliability of the fluid-dynamic model, we first performed test computations for simple physical situations. We considered two types of elemental units of length $L(= L_{\mathrm{I}} + L_{\mathrm{II}})$, say type 1 and 2, with a piecewise linear distribution of wall temperature, as depicted in Fig. 6. The unit is filled with a single-species gas. Assuming the periodic condition at the left and right ends of the unit, which is equivalent to considering an infinite connection of units ($\mathcal{N} = \infty$), we compute the induced particle flux N_f in a steady state by means of two different approaches: the computation of the fluid-dynamic model by the finite-difference method and that of the Boltzmann system by Bird's direct simulation Monte Carlo (DSMC) method [40,41]. In both computations, the hard-sphere molecular model is assumed; in the former approach, the *diffusion coefficients* $\mathcal{M}_{\mathrm{P}}$ and $\mathcal{M}_{\mathrm{T}}$ are computed by interpolation from the data in Ref. [42] that were obtained by accurate finite-difference analyses of the linearized Boltzmann equation. The computations were performed for $\mathrm{K}_* = 0.1$ in the case of type 1 and for $\mathrm{K}_* = 0.5$ in the case of type 2. Here, the reference Knudsen number $\mathrm{K}_* = \ell_*/D_*$ is defined with D_* being D_{I} and with n_* in Eq. (8) being the average number density of the gas.

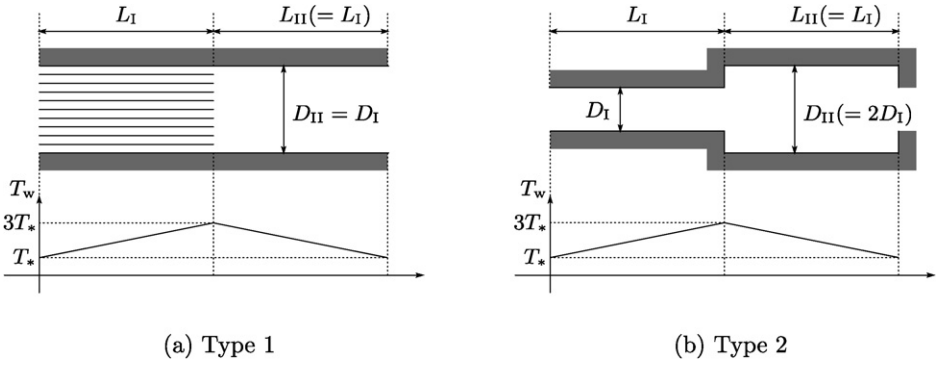

Fig. 6. Schematic of two types of elemental units and the distributions of wall temperature for test computations. (a) Type 1: $D_{\mathrm{II}}/D_{\mathrm{I}} = 1$, $L_{\mathrm{II}}/L_{\mathrm{I}} = 1$ and $N = 10$. (b) Type 2: $D_{\mathrm{II}}/D_{\mathrm{I}} = 2$, $L_{\mathrm{II}}/L_{\mathrm{I}} = 1$ and $N = 1$.

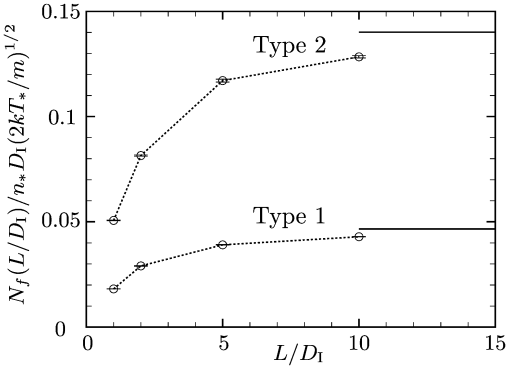

Fig. 7. Particle fluxes N_f induced in the units: type 1 and 2. The open circles with bars indicate the results of DSMC computation and their standard deviation. The solid lines indicate the results of the fluid-dynamic model ($L/D_\mathrm{I} \to \infty$). In the ordinate, m indicates the molecular mass of the gas.

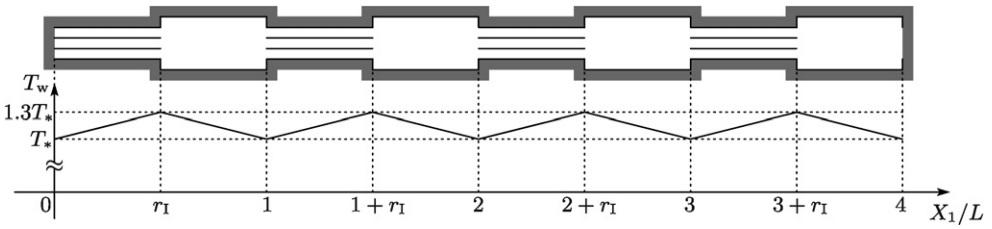

Fig. 8. Knudsen compressor and distribution of wall temperature used in the simulation in the case of $N = 3$ and $\mathcal{N} = 4$.

The particle fluxes obtained by the DSMC computations for several values of L/D_I are compared with those of the fluid-dynamic model in Fig. 7. In both cases, as L/D_I increases, the DSMC results approach those of the fluid-dynamic model, supporting that the fluid-dynamic model certainly provides an appropriate asymptotic limit as $L/D_\mathrm{I} \to \infty$ (or $\epsilon \to 0$). Further, it is seen from the figure that the fluid-dynamic model may be used as a practical model for $L/D_\mathrm{I} \gtrsim 10$.

5.2. Main results

In the present section, we shall present main results of the numerical simulations by the use of the fluid-dynamic model. We performed the simulations of the following scenario. Prepare a Knudsen compressor composed of $\mathcal{N}$ elemental units whose subunit I is subdivided into N channels of the same width ($a_1 = a_2 = \cdots = a_N$). With keeping the wall at a uniform temperature, which we shall take as the reference temperature T_*, put two different gases, gas A and B, of the same amount into the compressor. We shall take the average number density of the mixture in the compressor as the reference n_*. Close the both ends of the compressor, and, from a certain instant, set and keep the distribution of wall temperature piecewise linear as depicted in Fig. 8. Observe the behaviour of the mixture in a final steady state, especially the profiles of the pressure of the mixture and of the concentration of species A. The difference of the concentration from 0.5 is the measure of performance of the Knudsen compressor as a gas separator. In what follows, as in Section 5.1, D_I is taken as the reference D_*. It should be noted that the pressure and the concentration are common to the elements of subunit I, i.e., $\hat{p}_1 = \hat{p}_2 = \cdots = \hat{p}_N$ and $\chi_1^\mathrm{A} = \chi_2^\mathrm{A} = \cdots = \chi_N^\mathrm{A}$, because the subunit I is equally subdivided.

5.2.1. Numerical demonstration of the gas separation

We first present, in Fig. 9, a result of numerical simulation demonstrating the gas separation by means of the Knudsen compressor. In the simulation, the *diffusion coefficients* derived from the McCormack model [43] of the linearized Boltzmann equation for hard-sphere molecules (McCormack hard-sphere model) are used. The ratio of molecular mass $m^\mathrm{B}/m^\mathrm{A}$ and that of molecular diameter $d^\mathrm{B}/d^\mathrm{A}$ are, respectively, $m^\mathrm{B}/m^\mathrm{A} = 2$ and $d^\mathrm{B}/d^\mathrm{A} = 1$. In the figure, the profile of the pressure p of the mixture and that of the concentration χ^A of species A are shown by solid lines. In Fig. 9(a), the case of the 1-unit device, both the pressure and the concentration increase in subunit I

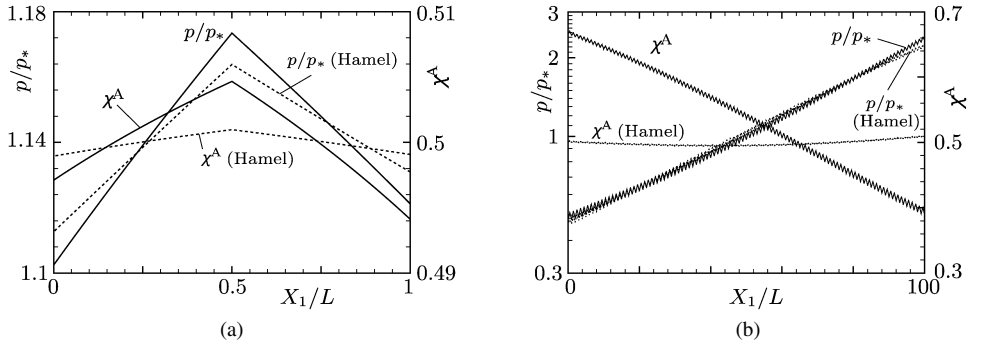

Fig. 9. Performance of the Knudsen compressor as a gas separator in the case of $\mathrm{K}_* = 1$, $r_{\mathrm{I}} = 0.5$, $N = 1$ and $a_{\mathrm{II}} = 2$. (a) Simulation of 1-unit device ($\mathcal{N} = 1$). (b) Simulation of 100-unit device ($\mathcal{N} = 100$). The solid lines indicate the results for the McCormack hard-sphere model, while the dashed lines with label "(Hamel)" those for the Hamel BGK-type model.

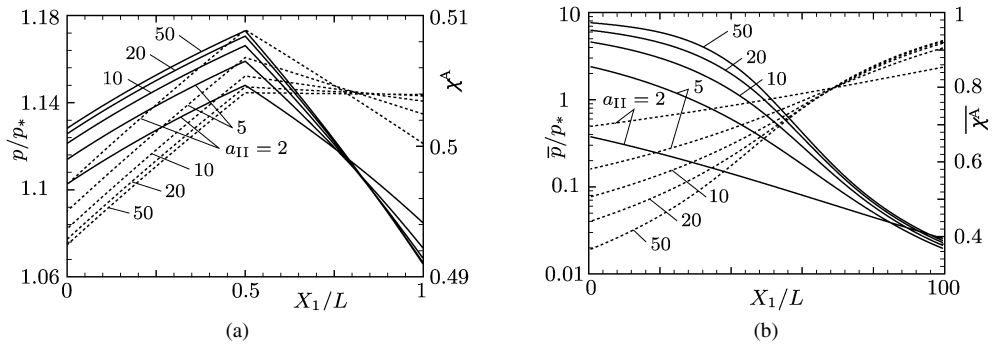

Fig. 10. Influence of the width of subunit II on the performance in the case of $\mathrm{K}_* = 1$, $r_{\mathrm{I}} = 0.5$ and $N = 1$. (a) Simulation of 1-unit device ($\mathcal{N} = 1$). (b) Simulation of 100-unit device ($\mathcal{N} = 100$). The solid lines indicate the profiles of the concentration of species A, while the dashed lines those of the pressure of the mixture. In (b), the pressure and concentration averaged in each unit, $\overline{p}$ and $\overline{\chi^{\mathrm{A}}}$, are shown at the middle point of each unit.

($0 < X_1/L < 0.5$) and decrease in subunit II ($0.5 < X_1/L < 1$). The differences of their values between the left and right ends are the measure of performance of the 1-unit device as a compressor and as a gas separator. As is obvious, the performance of the 1-unit device is very small. However, the performance can reach a practical level by increasing the number of units. The performance of the 100-unit device is shown in Fig. 9(b). In each elemental unit, the pressure p and the concentration χ^{A} behave similar to those in Fig. 9(a), leading to the zigzag distributions in Fig. 9(b). This figure demonstrates that the performance of the 100-unit device at practical level is due to the accumulation of the small effect in each elemental unit.

In the meantime, we performed the same simulation by the use of the *diffusion coefficients* obtained by the Hamel BGK-type model Boltzmann equation [44]. The parameters related to molecules are set $m^B/m^A = 2$ and $K^{\mathrm{BB}} = K^{\mathrm{BA}} = 1$. The results of the simulation are also shown in Fig. 9 by dashed lines with label "(Hamel)." Surprisingly, even the 100-unit device hardly works at all as a gas separator in spite that the performance as a compressor is almost the same. This result gives rise a question to the reliability of the simulation results for the McCormack hard-sphere model. However, from a certain physical reason and simulation results for other molecular models to be presented later, the BGK-type model is to be revealed inappropriate for the simulation of gas separation. For the moment, we shall leave the question open and continue to use the McCormack hard-sphere model in Section 5.2.2. We shall come back to the subject, the discussions on a proper modelling at the kinetic level, in Section 5.2.3.

5.2.2. Influence of the device geometry on the performance

By the use of the McCormack hard-sphere model with $m^{\mathrm{B}}/m^{\mathrm{A}} = 2$ and $d^{\mathrm{B}}/d^{\mathrm{A}} = 1$, we examine the influence of the geometry of the elemental unit on the performance of the device; the influence of the width of subunit II (or the ratio a_{II} of the width of subunit II to that of I) is shown in Fig. 10, that of the number N of subdivisions in subunit I in Fig. 11 and that of the proportion r_{I} of subunit I to the elemental unit in Fig. 12. In these figures, the profiles of

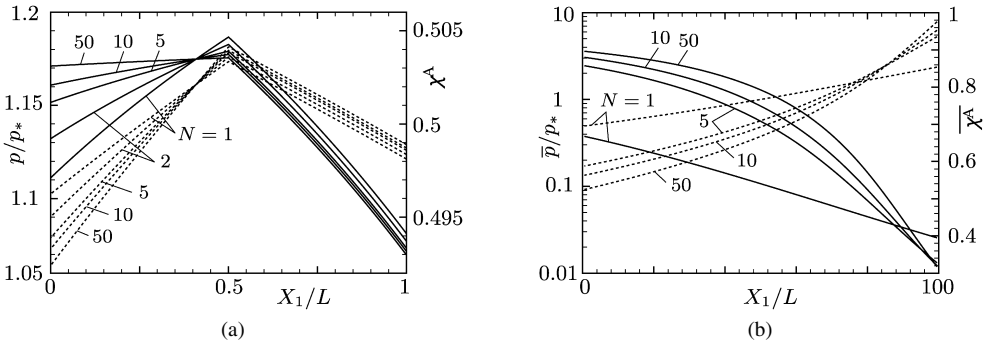

Fig. 11. Influence of the number of subdivisions in subunit I on the performance in the case of $\mathrm{K}_* = 1$, $r_{\mathrm{I}} = 0.5$ and $a_{\mathrm{II}} = 2$. (a) Simulation of 1-unit device ($\mathcal{N} = 1$). (b) Simulation of 100-unit device ($\mathcal{N} = 100$). See the caption of Fig. 10.

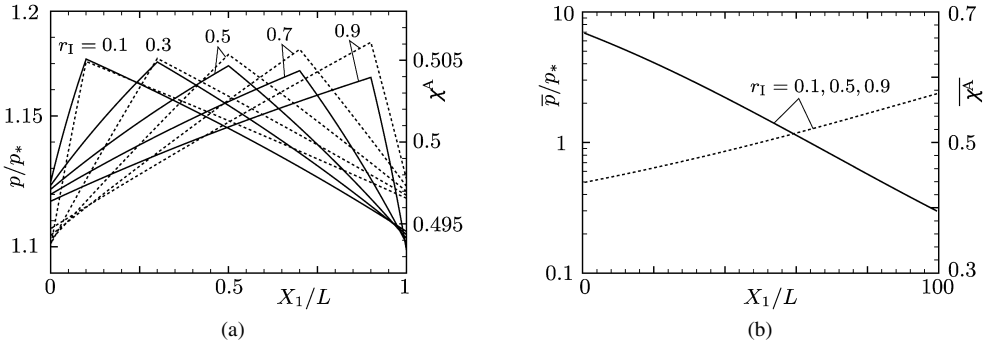

Fig. 12. Influence of the proportion of subunit I in elemental unit on the performance in the case of $\mathrm{K}_* = 1$, $N = 1$ and $a_{\mathrm{II}} = 2$. (a) Simulation of 1-unit device ($\mathcal{N} = 1$). (b) Simulation of 100-unit device ($\mathcal{N} = 100$). See the caption of Fig. 10.

the pressure and the concentration in the 100-unit device are not directly drawn; instead, their values averaged in each unit, which are denoted by $\overline{p}$ and $\overline{\chi^{\mathrm{A}}}$, are plotted at the middle point of each unit. The performance improves as a_{II} or N increases, while there is almost no influence of the proportion r_{I} of subunit I on the performance both as a compressor and as a gas separator. In Section 5.2.3, we shall present the simulation results for the case of $N = 5$, $a_{\mathrm{II}} = 5$ and $r_{\mathrm{I}} = 0.5$ for the study of the proper modelling at the kinetic level.

5.2.3. Proper modelling at the kinetic level

As is pointed out at the end of Section 5.2.1, the evaluation of the gas separation performance strongly depends on the choice of the kinetic model: the McCormack hard-sphere model yields prospective results, while the Hamel BGK-type model negative ones. We shall discuss the dependence of the gas separation performance on the modelling at the kinetic (or microscopic) level.

We consider three types of binary mixtures of noble gases, i.e., He–Ar, He–Ne and Ne–Ar, and investigate the behaviour of the mixtures on the basis of the McCormack equation for hard-sphere molecules, for the Maxwell molecules (McCormack Maxwell model), for the inverse power-law potential (McCormack IPL model) and for the Lennard-Jones 12,6 model (McCormack LJ model). Among these four models, the last is empirically most reliable and sometimes called the *realistic model*. The molar weights of He, Ne and Ar atoms are, respectively, 4.003, 20.183 and 39.944. The data of the parameters of molecular interactions, which are mainly taken from Ref. [45], are summarized in Table 1 (see also Appendices A.2.1–A.2.4). In the case of the Maxwell, IPL and LJ models, the parameters of the same-species interaction are determined from the viscosity μ and those of the different-species interaction are from the mutual diffusion coefficient D_{12}. In the case of the hard-sphere model, all the parameters are from the viscosity. (More precisely, the first approximations $[\mu]_1$ and $[D_{12}]_1$ in Chapman and Cowling [45] are used). In the simulations, the reference temperature T_* is commonly set as $T_* = 273$ K, while the reference Knudsen number K_* is set as $\mathrm{K}_* = 1$ (LJ), 1.52 (hard sphere), 1.10 (Maxwell) and 1.17 (IPL) in the case of the He–Ar and He–Ne mixtures and $\mathrm{K}_* = 1$ (LJ), 1.16 (hard sphere), 0.837 (Maxwell) and 0.889 (IPL) in the case of the Ne–Ar mixture. These values

Table 1
Data of molecular interactions between noble gases used in the present work

species α–β	$d^{\alpha\beta} \times 10^8$ (cm)	$d_*^{\alpha\beta} \times 10^8$ (cm)			$\nu^{\alpha\beta}$	$\frac{\epsilon^{\alpha\beta}}{k}$ (K)
	hard sphere	Maxwell	IPL	LJ	IPL	LJ
He–He	2.193[a]	2.58	2.50	2.70[b]	13.7[c]	6.03[b]
Ne–Ne	2.602[a]	3.06	2.97	2.80[b]	13.4[c]	35.7[b]
Ar–Ar	3.659[a]	4.30	4.32	3.42[b]	7.5[c]	124[b]
He–Ne	2.40[d]	3.00	2.74	2.64[e]	13.55[f]	23.7[e]
He–Ar	2.93[d]	3.50	3.32	2.98[e]	9.6[f]	40.2[e]
Ne–Ar	3.13[d]	3.85	3.66	3.11[e]	9.53[f]	61.7[e]

[a] In the fourth column of Table 11 in Ref. [45], p. 228.
[b] In the second or third column of Table 17 in Ref. [45], p. 237.
[c] In the third column of Table 14 in Ref. [45], p. 232.
[d] In the fifth column of Table 22 in Ref. [45], p. 263. Data by the rule of $d^{\alpha\beta} = (d^{\alpha\alpha} + d^{\beta\beta})/2$.
[e] In the sixth or seventh column of Table 23 in Ref. [45], p. 265.
[f] Data by the rule of $-1 + 2(\nu^{\alpha\alpha}\nu^{\beta\beta} - 1)/(\nu^{\alpha\alpha} + \nu^{\beta\beta} - 2)$. This is often used in the literature when experimental data is not available.

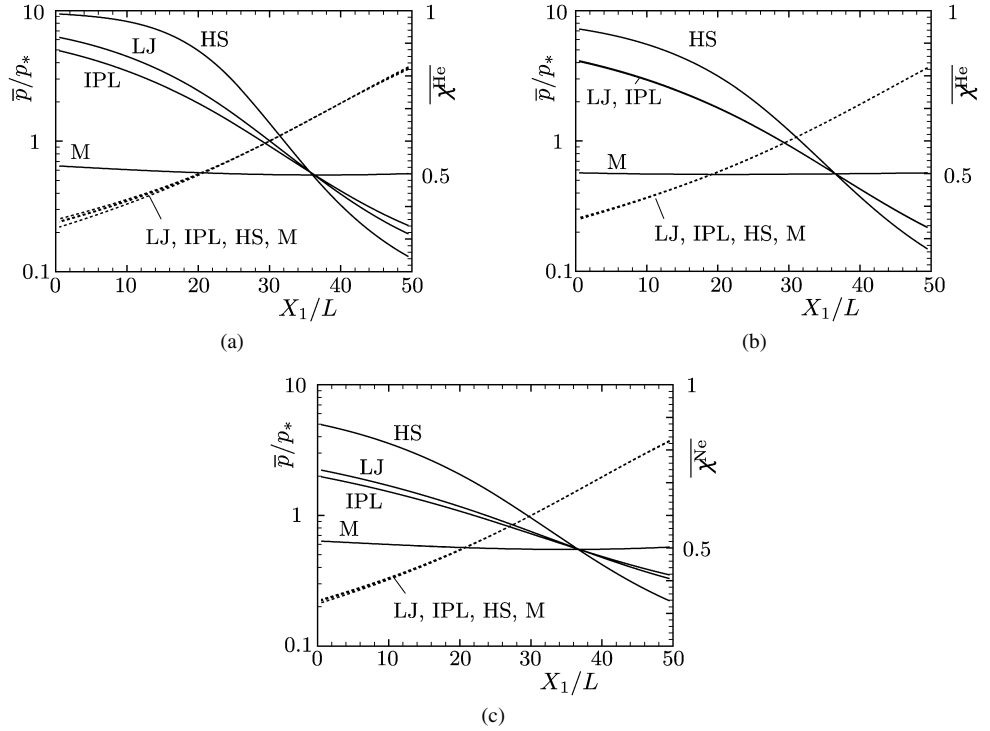

Fig. 13. Molecular model dependence of the performance of the 50-unit device for noble gas mixtures in the case of K_*(LJ model) = 1, $r_I = 0.5$, $N = 5$ and $a_{II} = 5$. (a) He–Ar, (b) He–Ne and (c) Ne–Ar. In (a) and (b) the solid lines indicate the concentration of He averaged in each unit, while in (c) they indicate the concentration of Ne averaged in each unit. The dashed lines indicate the pressure of the mixture averaged in each unit. The labels HS, LJ, IPL and M indicate the results for the McCormack hard-sphere, LJ, IPL and Maxwell models, respectively.

of K_* are chosen in order that the same experiment (see the scenario in Section 5.2) is simulated by the different kinetic models. (The superficial difference of the Knudsen number K_* comes from the difference of the definition of the mean free path among molecular models.) The results of the numerical simulations are shown in Fig. 13.

As is clear from the figure, the four models yield almost the same result for the performance as a compressor, while they give considerably different ones for the performance as a gas separator. Since the LJ model is expected to be reliable, we conclude that

(i) The modelling by the use of the Maxwell molecule or the (Hamel) BGK-type equation fails to capture the physical phenomenon of the gas separation. This modelling is unsuitable for the study of the gas separation in the Knudsen compressor.
(ii) The modelling by the use of the hard-sphere model exaggerates the gas separation effect to some extent but captures the qualitative feature well. This modelling is superior to that by the Maxwell molecule.
(iii) The results of the modelling by the use of the inverse power-law potential reasonably agree with those of the modelling by the Lennard-Jones model. Practically, the IPL modelling would be good enough for the performance estimate.

The incapability of the modelling by the Maxwell molecule reminds us that this model does not reproduce the so-called *thermal diffusion* [45–47], which is the diffusion caused by the gradient of the temperature in the fluid-dynamic regime. Since the source of the driving force of the Knudsen compressor is the temperature distribution on the device wall, the nonuniform concentration in the device can be explained by the thermal diffusion in the near fluid-dynamic regime (small K or K_*). This clearly explains why the modelling by the Maxwell molecule fails in this regime. However, in the rarefied regime, the relative motion of one to the other species is induced thermally even in the case of the Maxwell molecule. Thus, it is not obvious whether the feature in the fluid-dynamic regime is kept as the gas rarefaction increases. In this sense, the incapability of the Maxwell molecule in the entire range of the Knudsen number is one of the interesting findings in the present work. Incidentally, the BGK-type relaxation models, including the Hamel equation, are made in such a way that the momentum exchange between different species is the same as that of the Boltzmann equation for the Maxwell molecules. Therefore, the incapability of the Hamel equation in Fig. 9 may be considered to come from the properties of the Maxwell molecule described above.

6. Concluding remarks

We investigated a possibility of making use of the Knudsen compressor as a gas separator. Starting from the description at the microscopic level on the basis of the kinetic theory of gases, we first derived the fluid-dynamic model describing the behaviour of the mixture in the Knudsen compressor, following the idea proposed by Aoki and Degond [16]. Then by the use of this model, we numerically demonstrated that the Knudsen compressor works certainly as a gas separator. The separation performance is shown to reach a practical level by increasing the number of units in the device.

Further, by testing various molecular models at the kinetic level, it is found that the modelling by the celebrated Maxwell molecule (or the BGK-type model equation) fails to capture the gas separation in the Knudsen compressor. This presents a remarkable contrast to the capability of the other fundamental model, the hard-sphere molecule, even though this model exaggerates the separation effect to some extent.

In the present paper, in order to demonstrate that the Knudsen compressor does work as a gas separator, we have restricted ourselves to the simplest situation where the mixture is composed of only two species of monatomic gases. It is, however, possible to apply the present approach to more complicated situations such as mixtures of more than two species, those of polyatomic gases, etc. These would be interesting issues of practical importance for future works. We also restricted ourselves to the investigation of the final steady state, but the study of the time evolution is also important to estimate the performance of the device for real applications. The presented fluid-dynamic model will also serve for the research in this direction.

In conclusion, we took the solid first step of the research of gas separation by means of the Knudsen compressor. Further investigations such as the time evolution, energy supply estimates, experimental verification, etc. will enrich our knowledge to develop the gas separation method using the Knudsen compressor and its variants.

Acknowledgements

The authors thank Professor Kazuo Aoki for his interest in the present work. They also thank Professor Pierre Degond for his helpful comments on the present work. S. T. and H. S. acknowledge the support for their visits to his group in Toulouse by the Japan–Europe Research Cooperative Program of the Japan Society for the Promotion of Science. The stay of S. K. in Toulouse is supported by the grant from the Kyoto University Foundation.

Appendix A. Diffusion coefficients and the modelling at the kinetic level

As is mentioned in Remark 4, in order to obtain the *diffusion coefficients* $\mathcal{M}_{\rm P}$, $\mathcal{M}_{\rm P}^{\rm A}$, $\mathcal{M}_{\rm T}$, $\mathcal{M}_{\rm T}^{\rm A}$, $\mathcal{M}_{\chi}$ and $\mathcal{M}_{\chi}^{\rm A}$, we have to solve the boundary-value problem of the linearized Boltzmann equation (23) for three elemental flows. Nowadays, as is reported in [22], the solutions of the original Boltzmann equation for these flows can be obtained with high accuracy. Nevertheless, it still requires time-consuming computations, and it is almost impossible to construct a database covering the entire ranges of the Knudsen number and of the concentration and a certain range of the temperature. Therefore, in the present work, we constructed the database by the use of the model Boltzmann equation in place of the original one. To be specific, we adopted the McCormack [43] and Hamel BGK-type [44] models.

The advantage of using the model equations is not limited to the reduction of computational costs in finite-difference analyses. The model equation can be reduced to the integral equation for macroscopic quantities [29,48], which allows us to perform the numerical computations with higher accuracy when the velocity distribution function abruptly changes in the velocity space (e.g. the Poiseuille flow for large Knudsen numbers [42,22]). Moreover, from this reduced equation, we can derive the explicit expressions for the asymptotic behaviour of the particle fluxes for large Knudsen numbers in the same way as in Refs. [33–35]. These advantages, together with the asymptotic theory for small Knudsen numbers established by Sone [49,50,19], enable us to construct the database covering the entire range of the Knudsen numbers. We will give the details of these analyses in a separate paper and briefly describe the models adopted in the present work in this appendix.

A.1. Hamel BGK-type model equation

The Hamel BGK-type model [44] is a BGK-type relaxation model of the nonlinear Boltzmann equation for gas mixtures the collision terms of which are given by

$$J^{\beta\alpha}\bigl(f^{\beta}, f^{\alpha}\bigr) = C^{\beta\alpha} n^{\beta}\left(n^{\alpha} M\left(\boldsymbol{\xi} - \boldsymbol{v}^{\beta\alpha}; \frac{m^{\alpha}}{2kT^{\beta\alpha}}\right) - f^{\alpha}\right),$$

$$\boldsymbol{v}^{\beta\alpha} = \frac{m^{\alpha}\boldsymbol{v}^{\alpha} + m^{\beta}\boldsymbol{v}^{\beta}}{m^{\alpha}+m^{\beta}}, \qquad T^{\beta\alpha} = T^{\alpha} + \frac{\mu^{\beta\alpha}}{m^{\alpha}+m^{\beta}}\left(T^{\beta} - T^{\alpha} + \frac{m^{\beta}}{6k}\bigl|\boldsymbol{v}^{\beta} - \boldsymbol{v}^{\alpha}\bigr|^2\right),$$

where n^{α}, $\boldsymbol{v}^{\alpha}$ and T^{α} are those defined by Eqs. (3)–(4) and $C^{\alpha\beta}$'s are constants with the symmetry $C^{\rm AB} = C^{\rm BA}$.

For this model, corresponding to Eq. (9), we define $B_*^{\beta\alpha}$ as

$$B_*^{\beta\alpha} = \frac{\sqrt{\pi}}{2} C^{\beta\alpha} \int M\left(\boldsymbol{\xi}; \frac{m^{\alpha}}{2kT_*}\right) \mathrm{d}^3\xi = \frac{\sqrt{\pi}}{2} C^{\beta\alpha},$$

so that

$$\ell_* = \frac{(8kT_*/m^{\rm A}\pi)^{1/2}}{n_* C^{\rm AA}}, \quad K^{\rm BB} = \frac{C^{\rm BB}}{C^{\rm AA}}, \quad K^{\rm AB} = K^{\rm BA} = \frac{C^{\rm BA}}{C^{\rm AA}}.$$

For the construction of the database of the *diffusion coefficients*, we need the linearized version of the collision terms, which is given by

$$L_{\widehat{T}_{\rm w}}^{\beta\alpha}\bigl(\chi_{(0)}^{\alpha}\phi^{\beta}, \chi_{(0)}^{\beta}\phi^{\alpha}\bigr) = \frac{2}{\sqrt{\pi}}\frac{\hat{n}_{(0)}}{\sqrt{\widehat{T}_{\rm w}}}\chi_{(0)}^{\beta}\bigl(h^{\beta\alpha} - \phi^{\alpha}\bigr),$$

$$h^{\beta\alpha} = \omega^{\alpha} + 2\widehat{m}^{\alpha}\chi_{(0)}^{\alpha} c_i u_i^{\beta\alpha} + \left(\widehat{m}^{\alpha}|\boldsymbol{c}|^2 - \frac{3}{2}\right)\chi_{(0)}^{\alpha}\theta^{\beta\alpha},$$

$$u_i^{\beta\alpha} = \frac{\widehat{m}^{\alpha}u_i^{\alpha} + \widehat{m}^{\beta}u_i^{\beta}}{\widehat{m}^{\alpha}+\widehat{m}^{\beta}}, \qquad \theta^{\beta\alpha} = \theta^{\alpha} + \frac{1}{2}\frac{\hat{\mu}^{\beta\alpha}}{\widehat{m}^{\alpha}}\frac{\hat{\mu}^{\beta\alpha}}{\widehat{m}^{\beta}}\bigl(\theta^{\beta} - \theta^{\alpha}\bigr),$$

$$\omega^{\alpha} = \int \phi^{\alpha} M\bigl(\boldsymbol{c}; \widehat{m}^{\alpha}\bigr)\,\mathrm{d}^3c, \qquad u_i^{\alpha} = \frac{1}{\chi_{(0)}^{\alpha}}\int c_i\phi^{\alpha} M\bigl(\boldsymbol{c}; \widehat{m}^{\alpha}\bigr)\,\mathrm{d}^3c,$$

$$\theta^{\alpha} = \frac{2}{3\chi_{(0)}^{\alpha}}\int\left(\widehat{m}^{\alpha}|\boldsymbol{c}|^2 - \frac{3}{2}\right)\phi^{\alpha} M\bigl(\boldsymbol{c}; \widehat{m}^{\alpha}\bigr)\,\mathrm{d}^3c.$$

Note the simple and explicit dependence of $L^{\beta\alpha}_{\widehat{T}_{\rm w}}$ on $\widehat{T}_{\rm w}$. Because of this simplicity, one may construct the database only for $\widehat{T}_{\rm w}=1$, and the *diffusion coefficients* for $\widehat{T}_{\rm w}\neq 1$ can be obtained by the relation

$$\mathcal{M}\big(\mathrm{K},\chi^{\rm A}_{(0)},\widehat{T}_{\rm w}\big)=\mathcal{M}\big(\mathrm{K}\sqrt{\widehat{T}_{\rm w}},\chi^{\rm A}_{(0)},1\big),$$

where $\mathcal{M}$ represents $\mathcal{M}_{\rm P}$, $\mathcal{M}^{\rm A}_{\rm P}$, $\mathcal{M}_{\rm T}$, $\mathcal{M}^{\rm A}_{\rm T}$, $\mathcal{M}_{\chi}$ and $\mathcal{M}^{\rm A}_{\chi}$.

A.2. McCormack model equation

The McCormack model [43] is a model of the linearized Boltzmann equation for gas mixtures obtained by the approximation in terms of a complete orthogonal set of functions. The model adopted here is the so-called third-order model, which reads, in the dimensionless form,

$$\begin{aligned}
&L^{\beta\alpha}_{\widehat{T}_{\rm w}}\big(\chi^{\alpha}_{(0)}\phi^{\beta},\chi^{\beta}_{(0)}\phi^{\alpha}\big)=M^{\beta\alpha}-C^{\beta\alpha}\phi^{\alpha},\\
&M^{\beta\alpha}=C^{\beta\alpha}\omega^{\alpha}+2\widehat{m}^{\alpha}c_i\bigg[C^{\beta\alpha}\chi^{\alpha}_{(0)}u^{\alpha}_i+\chi^{\alpha}_{(0)}\chi^{\beta}_{(0)}\big(u^{\beta}_i-u^{\alpha}_i\big)\nu^{(1)}_{\beta\alpha}+\bigg(\frac{\chi^{\alpha}_{(0)}Q^{\beta}_i}{\widehat{m}^{\beta}}-\frac{\chi^{\beta}_{(0)}Q^{\alpha}_i}{\widehat{m}^{\alpha}}\bigg)\nu^{(2)}_{\beta\alpha}\bigg]\\
&\qquad+\chi^{\alpha}_{(0)}\bigg(\widehat{m}^{\alpha}|\boldsymbol{c}|^2-\frac{3}{2}\bigg)\bigg(C^{\beta\alpha}\theta^{\alpha}+\frac{\hat{\mu}^{\beta\alpha}}{\widehat{m}^{\beta}}\big(\theta^{\beta}-\theta^{\alpha}\big)\chi^{\beta}_{(0)}\nu^{(1)}_{\beta\alpha}\bigg)\\
&\qquad+\widehat{m}^{\alpha}\bigg(c_ic_j-\frac{1}{3}|\boldsymbol{c}|^2\delta_{ij}\bigg)\big(\big(C^{\beta\alpha}-\chi^{\beta}_{(0)}\nu^{(3)}_{\beta\alpha}\big)P^{\alpha}_{ij}+\chi^{\alpha}_{(0)}\nu^{(4)}_{\beta\alpha}P^{\beta}_{ij}\big)\\
&\qquad+\frac{4}{5}\widehat{m}^{\alpha}c_i\bigg(\widehat{m}^{\alpha}|\boldsymbol{c}|^2-\frac{5}{2}\bigg)\bigg(\big(C^{\beta\alpha}-\chi^{\beta}_{(0)}\nu^{(5)}_{\beta\alpha}\big)Q^{\alpha}_i+\chi^{\alpha}_{(0)}\nu^{(6)}_{\beta\alpha}Q^{\beta}_i+\frac{5}{2}\frac{\chi^{\alpha}_{(0)}\chi^{\beta}_{(0)}}{\widehat{m}^{\alpha}}\big(u^{\beta}_i-u^{\alpha}_i\big)\nu^{(2)}_{\beta\alpha}\bigg),
\end{aligned}$$

where ω^{α}, u^{α}_i and θ^{α} are the same as those in the Hamel model,

$$\begin{aligned}
&P^{\alpha}_{ij}=2\widehat{m}^{\alpha}\int c_ic_j\phi^{\alpha}M\big(\boldsymbol{c};\widehat{m}^{\alpha}\big)\,\mathrm{d}^3c,\\
&Q^{\alpha}_i=\int c_i\bigg(\widehat{m}^{\alpha}|\boldsymbol{c}|^2-\frac{5}{2}\bigg)\phi^{\alpha}M\big(\boldsymbol{c};\widehat{m}^{\alpha}\big)\,\mathrm{d}^3c,
\end{aligned}$$

and

$$\begin{aligned}
&\nu^{(1)}_{\beta\alpha}=\frac{8}{3}\frac{\hat{\mu}^{\beta\alpha}}{\widehat{m}^{\alpha}}\Omega^{\beta\alpha}_{11}\big(\widehat{T}_{\rm w}\big),\qquad \nu^{(2)}_{\beta\alpha}=\frac{\hat{\mu}^{\beta\alpha}}{5}\bigg(\frac{8}{3}\frac{\hat{\mu}^{\beta\alpha}}{\widehat{m}^{\alpha}}\Omega^{\beta\alpha}_{12}\big(\widehat{T}_{\rm w}\big)-\frac{5}{2}\nu^{(1)}_{\beta\alpha}\bigg),\\
&\nu^{(3)}_{\beta\alpha}=\frac{\hat{\mu}^{\beta\alpha}}{\widehat{m}^{\alpha}}\bigg(\frac{4}{5}\frac{\hat{\mu}^{\beta\alpha}}{\widehat{m}^{\alpha}}\Omega^{\beta\alpha}_{22}\big(\widehat{T}_{\rm w}\big)+\frac{\widehat{m}^{\alpha}}{\widehat{m}^{\beta}}\nu^{(1)}_{\beta\alpha}\bigg),\qquad \nu^{(4)}_{\beta\alpha}=\frac{\widehat{m}^{\alpha}}{\widehat{m}^{\beta}}\big(2\nu^{(1)}_{\beta\alpha}-\nu^{(3)}_{\beta\alpha}\big),\\
&\nu^{(5)}_{\beta\alpha}=\frac{8}{15}\bigg(\frac{\hat{\mu}^{\beta\alpha}}{\widehat{m}^{\alpha}}\bigg)^3\frac{\widehat{m}^{\alpha}}{\widehat{m}^{\beta}}\bigg[\Omega^{\beta\alpha}_{22}\big(\widehat{T}_{\rm w}\big)+\bigg(\frac{15}{4}\frac{\widehat{m}^{\alpha}}{\widehat{m}^{\beta}}+\frac{25}{8}\frac{\widehat{m}^{\beta}}{\widehat{m}^{\alpha}}\bigg)\Omega^{\beta\alpha}_{11}\big(\widehat{T}_{\rm w}\big)-\frac{1}{2}\frac{\widehat{m}^{\beta}}{\widehat{m}^{\alpha}}\Big(5\Omega^{\beta\alpha}_{12}\big(\widehat{T}_{\rm w}\big)-\Omega^{\beta\alpha}_{13}\big(\widehat{T}_{\rm w}\big)\Big)\bigg],\\
&\nu^{(6)}_{\beta\alpha}=\frac{8}{15}\bigg(\frac{\hat{\mu}^{\beta\alpha}}{\widehat{m}^{\alpha}}\bigg)^3\frac{\widehat{m}^{\alpha}}{\widehat{m}^{\beta}}\bigg[-\Omega^{\beta\alpha}_{22}\big(\widehat{T}_{\rm w}\big)+\frac{55}{8}\Omega^{\beta\alpha}_{11}\big(\widehat{T}_{\rm w}\big)-\frac{5}{2}\Omega^{\beta\alpha}_{12}\big(\widehat{T}_{\rm w}\big)+\frac{1}{2}\Omega^{\beta\alpha}_{13}\big(\widehat{T}_{\rm w}\big)\bigg],
\end{aligned}$$

with $\Omega^{\beta\alpha}_{kl}$ being the function defined as

$$\begin{aligned}
&\Omega^{\beta\alpha}_{kl}(\tau)=\bigg(\frac{\hat{\mu}^{\beta\alpha}}{2}\bigg)^{l+3/2}\int_0^{\infty}\exp\bigg(-\frac{\hat{\mu}^{\beta\alpha}}{2}z^2\bigg)z^{2l+2}\Lambda^{\beta\alpha}_k(z,\tau)\,\mathrm{d}z,\\
&\Lambda^{\beta\alpha}_k(z,\tau)=2\sqrt{\pi}\int_0^{\pi/2}b^{\beta\alpha}_{\tau}(\cos\theta,z)\big[1-\cos^k(\pi-2\theta)\big]\sin\theta\,\mathrm{d}\theta.
\end{aligned}$$

Here $C^{\beta\alpha}$'s are constants with respect to $\boldsymbol{c}$ and occur in the total collision integral $\sum_{\beta=\mathrm{A,B}} K^{\beta\alpha} L^{\beta\alpha}_{\widehat{T}_\mathrm{w}}$ (for species α) not separately but in the combination of $K^{\mathrm{A}\alpha} C^{\mathrm{A}\alpha} + K^{\mathrm{B}\alpha} C^{\mathrm{B}\alpha}$. We denote this combination by C^α and, following the choice by Cercignani and Sharipov [51], define it as

$$C^\mathrm{A} = \frac{\sqrt{\pi}}{2} \frac{\Psi^\mathrm{A}\Psi^\mathrm{B} - \chi^\mathrm{A}_{(0)}\chi^\mathrm{B}_{(0)}\nu^{(4)}_\mathrm{AB}\nu^{(4)}_\mathrm{BA}(K^\mathrm{BA})^2}{\Psi^\mathrm{B} + \chi^\mathrm{B}_{(0)}\nu^{(4)}_\mathrm{BA}K^\mathrm{BA}}, \qquad C^\mathrm{B} = \frac{\Psi^\mathrm{B} + \chi^\mathrm{B}_{(0)}\nu^{(4)}_\mathrm{BA}K^\mathrm{BA}}{\Psi^\mathrm{A} + \chi^\mathrm{A}_{(0)}\nu^{(4)}_\mathrm{AB}K^\mathrm{AB}} C^\mathrm{A},$$

with

$$\Psi^\mathrm{A} = \chi^\mathrm{A}_{(0)}K^\mathrm{AA}\big(\nu^{(3)}_\mathrm{AA} - \nu^{(4)}_\mathrm{AA}\big) + \chi^\mathrm{B}_{(0)}K^\mathrm{BA}\nu^{(3)}_\mathrm{BA}, \qquad \Psi^\mathrm{B} = \chi^\mathrm{B}_{(0)}K^\mathrm{BB}\big(\nu^{(3)}_\mathrm{BB} - \nu^{(4)}_\mathrm{BB}\big) + \chi^\mathrm{A}_{(0)}K^\mathrm{AB}\nu^{(3)}_\mathrm{AB}.$$

As is clear from the definition above, a specific form of $b^{\beta\alpha}_{\widehat{T}_\mathrm{w}}$ is necessary to complete the model. In this sense, the McCormack model can be adapted to various specific molecular models. We shall give below the information about the molecular models used in the present work.

A.2.1. Hard-sphere model

Denoting the molecular diameter of species α by d^α, the function $B^{\beta\alpha}$ representing the molecular interaction for hard-sphere molecules is written as

$$B^{\beta\alpha}\left(\frac{|\boldsymbol{e}\cdot\boldsymbol{V}|}{|\boldsymbol{V}|}, |\boldsymbol{V}|\right) = \frac{1}{2}\big(d^{\beta\alpha}\big)^2|\boldsymbol{V}\cdot\boldsymbol{e}|, \quad d^{\beta\alpha} = \frac{d^\alpha + d^\beta}{2}.$$

From this, $B^{\beta\alpha}_*$'s are given by

$$B^{\beta\alpha}_* = \pi\left(\frac{2}{\hat{\mu}^{\beta\alpha}}\right)^{1/2}\big(d^{\beta\alpha}\big)^2\left(\frac{2kT_*}{m^\mathrm{A}}\right)^{1/2},$$

and the reference mean free path ℓ_*, the coefficients $K^{\beta\alpha}$'s and the function $b^{\beta\alpha}_\tau$ are expressed as

$$\ell_* = \frac{1}{\sqrt{2}\pi(d^\mathrm{A})^2 n_*},$$

$$K^\mathrm{BB} = \left(\frac{d^\mathrm{B}}{d^\mathrm{A}}\right)^2\left(\frac{m^\mathrm{A}}{m^\mathrm{B}}\right)^{1/2}, \qquad K^\mathrm{AB} = K^\mathrm{BA} = \left(\frac{d^\mathrm{BA}}{d^\mathrm{A}}\right)^2\left(\frac{1}{\hat{\mu}^\mathrm{BA}}\right)^{1/2},$$

$$b^{\beta\alpha}_\tau\left(\frac{|\boldsymbol{e}\cdot\boldsymbol{C}|}{|\boldsymbol{C}|}, |\boldsymbol{C}|\right) = \frac{1}{2\pi}\left(\frac{\hat{\mu}^{\beta\alpha}}{2}\right)^{1/2}|\boldsymbol{C}\cdot\boldsymbol{e}|.$$

It should be noted that $b^{\beta\alpha}_{\widehat{T}_\mathrm{w}}$ does not depend on $\widehat{T}_\mathrm{w}$, so that the same is true for the *diffusion coefficients*:

$$\mathcal{M}\big(\mathrm{K}, \chi^\mathrm{A}_{(0)}, \widehat{T}_\mathrm{w}\big) = \mathcal{M}\big(\mathrm{K}, \chi^\mathrm{A}_{(0)}, 1\big),$$

where $\mathcal{M}$ represents $\mathcal{M}_\mathrm{P}$, $\mathcal{M}^\mathrm{A}_\mathrm{P}$, $\mathcal{M}_\mathrm{T}$, $\mathcal{M}^\mathrm{A}_\mathrm{T}$, $\mathcal{M}_\chi$ and $\mathcal{M}^\mathrm{A}_\chi$. This property, as in the case of the Hamel model equation, reduces the computational cost for the database construction. Incidentally, $\Omega^{\beta\alpha}_{kl}$ is expressed as

$$\Omega^{\beta\alpha}_{kl}(\tau) = \frac{1}{8\sqrt{\pi}}\left(2 - \frac{1+(-1)^k}{k+1}\right)(l+1)!,$$

and is independent of τ.

A.2.2. Inverse power-law potential model

This model assumes the molecular interaction between species α and β with the potential $U^{\beta\alpha}$ of repulsive central force given by

$$U^{\beta\alpha}(r) = \frac{a^{\beta\alpha}}{r^{\nu^{\beta\alpha}-1}}, \qquad \nu^{\beta\alpha} \geqslant 3,$$

where r is the distance between the centres of molecules and $a^{\beta\alpha}$ is a positive constant. For this model, the function $B^{\beta\alpha}$ is written as

$$B^{\beta\alpha}\bigl(\cos\theta, |\boldsymbol{V}|\bigr) = \frac{1}{2}\left(\frac{4a^{\beta\alpha}}{\mu^{\beta\alpha}}\right)^{2/(\nu^{\beta\alpha}-1)} |\boldsymbol{V}|^{(\nu^{\beta\alpha}-5)/(\nu^{\beta\alpha}-1)} \frac{g(\theta)}{\sin\theta}\frac{\mathrm{d}g}{\mathrm{d}\theta} \quad \left(0 < \theta < \frac{\pi}{2}\right),$$

where g is the monotonically increasing function of θ defined by the integral

$$\theta = \int_0^{y_c(g)} \left[1 - \left(\frac{y}{g}\right)^{\nu^{\beta\alpha}-1} - y^2\right]^{-1/2} \mathrm{d}y,$$

with y_c being the (unique) positive solution of the equation $1 - (y/g)^{\nu^{\beta\alpha}-1} - y^2 = 0$. Since the integral in Eq. (9) diverges for this $B^{\beta\alpha}$, we define $B_*^{\beta\alpha}$'s alternatively by

$$B_*^{\beta\alpha} = \pi\left(\frac{2}{\hat{\mu}^{\beta\alpha}}\right)^{1/2} \bigl(d_*^{\beta\alpha}\bigr)^2 \left(\frac{2kT_*}{m^{\mathrm{A}}}\right)^{1/2},$$

where

$$d_*^{\beta\alpha} = \left(\frac{(\nu^{\beta\alpha}-1)a^{\beta\alpha}}{2kT_*}\right)^{1/(\nu^{\beta\alpha}-1)}.$$

This $d_*^{\beta\alpha}$ has the dimension of length and a nice correspondence to the molecular diameter of the hard-sphere model (see Section 10.31 in Ref. [45] and Table 1). In fact, the reference mean free path ℓ_* and the coefficients $K^{\beta\alpha}$'s can be written by the same expressions as those of the hard-sphere model with $d^{\beta\alpha}$ being replaced by $d_*^{\beta\alpha}$. The function $b_\tau^{\beta\alpha}$ is written as

$$b_\tau^{\beta\alpha}\bigl(\cos\theta, |\boldsymbol{C}|\bigr) = \frac{1}{2\pi}\left(\frac{2}{(\nu^{\beta\alpha}-1)\tau}\right)^{2/(\nu^{\beta\alpha}-1)} \left(\frac{\hat{\mu}^{\beta\alpha}}{2}|\boldsymbol{C}|^2\right)^{(\nu^{\beta\alpha}-5)/(2(\nu^{\beta\alpha}-1))} \frac{g(\theta)}{\sin\theta}\frac{\mathrm{d}g}{\mathrm{d}\theta},$$

leading to the following expressions of $\Omega_{kl}^{\beta\alpha}$'s occurring in the model:

$$\Omega_{kl}^{\beta\alpha}(\tau) = \frac{1}{2\sqrt{\pi}}\,\tau^{-2/(\nu^{\beta\alpha}-1)} A_k\bigl(\nu^{\beta\alpha}\bigr)\Gamma\left(l + 2 - \frac{2}{\nu^{\beta\alpha}-1}\right).$$

Here $A_k(\nu^{\beta\alpha})$ is the function in Chapman and Cowling (Ref. [45], p. 171) and Γ the gamma function.

A.2.3. Maxwell molecule

The Maxwell molecular model is a special kind of the inverse power-law potential model whose exponents are commonly set as $\nu^{\beta\alpha} = 5$. This model has a celebrated feature that the dependence of $B^{\beta\alpha}$ on the relative speed between colliding molecules vanishes:

$$B^{\beta\alpha}\bigl(\cos\theta, |\boldsymbol{V}|\bigr) = \left(\frac{a^{\beta\alpha}}{\mu^{\beta\alpha}}\right)^{1/2} \frac{g(\theta)}{\sin\theta}\frac{\mathrm{d}g}{\mathrm{d}\theta} \quad \left(0 < \theta < \frac{\pi}{2}\right).$$

The expressions for $d_*^{\beta\alpha}$, $b_\tau^{\beta\alpha}$ and $\Omega_{kl}^{\beta\alpha}(\tau)$ are those in Section A.2.2 with $\nu^{\beta\alpha} = 5$. It should be noted that $\Omega_{kl}^{\beta\alpha}(\tau)$'s are commonly proportional to $\tau^{-1/2}$, so that one may construct the database of the *diffusion coefficients* only for $\widehat{T}_{\mathrm{w}} = 1$. The *diffusion coefficients* for $\widehat{T}_{\mathrm{w}} \neq 1$ can be obtained by the same relation as in the case of the Hamel model. This correspondence reflects the fact that the Hamel model is the relaxation model of the Boltzmann equation for the Maxwell molecules.

A.2.4. Lennard-Jones 12,6 model

This model assumes the molecular interaction between species β and α with the potential $U^{\beta\alpha}$ of the form

$$U^{\beta\alpha}(r) = 4\epsilon^{\beta\alpha}\left[\left(\frac{d_*^{\beta\alpha}}{r}\right)^{12} - \left(\frac{d_*^{\beta\alpha}}{r}\right)^{6}\right],$$

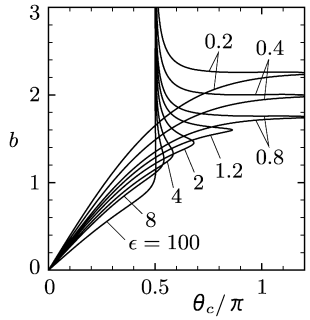

Fig. 14. Dimensionless impact parameter b vs. θ_c.

where r is the distance between the centres of molecules and $\epsilon^{\beta\alpha}$ and $d_*^{\beta\alpha}$ are positive constants. For this model, the positive function $B^{\beta\alpha}$ is written as

$$B^{\beta\alpha}\big(\cos\theta, |\boldsymbol{V}|\big) = \frac{1}{2}\big(d_*^{\beta\alpha}\big)^2 |\boldsymbol{V}| \frac{1}{\sin\theta} \sum_{\theta_c} b(\epsilon, \theta_c) \left|\frac{\partial b}{\partial \theta_c}\right| \quad \left(0 < \theta < \frac{\pi}{2}\right),$$

where $\epsilon = \mu^{\beta\alpha}|\boldsymbol{V}|^2/4\epsilon^{\beta\alpha}$ and $b(\geqslant 0)$ is the dimensionless impact parameter, which can be expressed as a function of ϵ and θ_c by the relation of implicit form

$$\theta_c = \frac{1}{2} b\sqrt{\epsilon} \int_0^{y_c(b,\epsilon)} \left[\frac{1}{4}\epsilon\big(1 - b^2 y^2\big) + y^6 - y^{12}\right]^{-1/2} \mathrm{d}y,$$

with y_c being the smallest positive solution of the equation $\frac{1}{4}\epsilon(1 - b^2y^2) + y^6 - y^{12} = 0$. The notation $\sum_{\theta_c}$ denotes that, for each fixed θ, the summation is taken over all the values of $\theta_c(\geqslant 0)$ such that $\theta_c = \theta + n\pi$ or $(n+1)\pi - \theta$ $(n = 0, 1, 2, \ldots)$. As is seen in Fig. 14, there are two different b's, say b_{small} and b_{large}, for every fixed θ_c and ϵ in the range $\theta_c > \pi/2$. In this range, the term $b|\partial b/\partial\theta_c|$ reads $b_{\mathrm{small}}|\partial b_{\mathrm{small}}/\partial\theta_c| + b_{\mathrm{large}}|\partial b_{\mathrm{large}}/\partial\theta_c|$.

As in the case of the inverse power-law potential model, the integral in Eq. (9) diverges for this $B^{\beta\alpha}$; thus we define $B_*^{\beta\alpha}$'s by

$$B_*^{\beta\alpha} = \pi\left(\frac{2}{\hat{\mu}^{\beta\alpha}}\right)^{1/2} \big(d_*^{\beta\alpha}\big)^2 \left(\frac{2kT_*}{m^{\mathrm{A}}}\right)^{1/2}.$$

Then the reference mean free path ℓ_* and the coefficients $K^{\beta\alpha}$'s can be written again by the same expressions as those of the hard-sphere model with $d^{\beta\alpha}$ being replaced by $d_*^{\beta\alpha}$. The function $b_\tau^{\beta\alpha}$ is written as

$$b_\tau^{\beta\alpha}\big(\cos\theta, |\boldsymbol{C}|\big) = \frac{1}{2\pi}\left(\frac{\hat{\mu}^{\beta\alpha}}{2}\right)^{1/2} |\boldsymbol{C}| \frac{1}{\sin\theta} \sum_{\theta_c} b(\epsilon, \theta_c) \left|\frac{\partial b}{\partial \theta_c}\right| \quad \left(0 < \theta < \frac{\pi}{2}\right),$$

with $\epsilon = \hat{\mu}^{\beta\alpha}|\boldsymbol{C}|^2 kT_*\tau/2\epsilon^{\beta\alpha}$. Since the integration in the definition of $\Lambda_k^{\beta\alpha}$'s cannot be carried out analytically for this $b_\tau^{\beta\alpha}$, we do not have explicit expressions for $\Omega_{kl}^{\beta\alpha}$'s and have their functional form only numerically.

References

[1] J.C. Maxwell, On stresses in rarefied gases arising from inequalities of temperature, Philos. Trans. Roy. Soc. 170 (1879) 231–256.
[2] M. Knudsen, Eine Revision Gleichgewichtsbedingung der Gase. Thermische Molekularströmung, Ann. Phys. (Leipzig) 31 (1910) 205–229.
[3] E.H. Kennard, Kinetic Theory of Gases, McGraw-Hill, New York, 1938.
[4] G. Pham-Van-Diep, P. Keeley, E.P. Muntz, D.P. Weaver, A micromechanical Knudsen compressor, in: J. Harvey, G. Lord (Eds.), Rarefied Gas Dynamics, vol. I, Oxford University Press, London, 1995, pp. 715–721.
[5] Y. Sone, Y. Waniguchi, K. Aoki, One-way flow of a rarefied gas induced in a channel with a periodic temperature distribution, Phys. Fluids 8 (1996) 2227–2235.

[6] S.E. Vargo, E.P. Muntz, An evaluation of a multiple-stage micromechanical Knudsen compressor and vacuum pump, in: C. Shen (Ed.), Rarefied Gas Dynamics, Peking University Press, Beijing, 1997, pp. 995–1000.
[7] M.L. Hudson, T.J. Bartel, DSMC simulation of thermal transpiration and accommodation pumps, in: R. Brun, R. Campargue, R. Gatignol, J.-C. Lengrand (Eds.), Rarefied Gas Dynamics, vol. 1, Cepadues, Toulouse, 1999, pp. 719–726.
[8] M. Young, Y.L. Han, E.P. Muntz, G. Shiflett, A. Ketsdever, A. Green, Thermal transpiration in microsphere membranes, in: A.D. Ketsdever, E.P. Muntz (Eds.), Rarefied Gas Dynamics, AIP, New York, 2003, pp. 743–751.
[9] Y.L. Han, M. Young, E.P. Muntz, G. Shiflett, Knudsen compressor performance at low pressures, in: M. Capitelli (Ed.), Rarefied Gas Dynamics, AIP, New York, 2005, pp. 162–167.
[10] M. Young, Y.L. Han, E.P. Muntz, G. Shiflett, Characterization and optimization of a radiantly driven multi-stage Knudsen compressor, in: M. Capitelli (Ed.), Rarefied Gas Dynamics, AIP, New York, 2005, pp. 174–179.
[11] Y. Sone, K. Sato, Demonstration of a one-way flow of a rarefied gas induced through a pipe without average pressure and temperature gradients, Phys. Fluids 12 (2000) 1864–1868.
[12] K. Aoki, Y. Sone, S. Takata, K. Takahashi, G.A. Bird, One-way flow of a rarefied gas induced in a circular pipe with a periodic temperature distribution, in: T.J. Bartel, M.A. Gallis (Eds.), Rarefied Gas Dynamics, AIP, New York, 2001, pp. 940–947.
[13] Y. Sone, T. Fukuda, T. Hokazono, H. Sugimoto, Experiment on a one-way flow of a rarefied gas through a straight circular pipe without average temperature and pressure gradients, in: T.J. Bartel, M.A. Gallis (Eds.), Rarefied Gas Dynamics, AIP, New York, 2001, pp. 948–955.
[14] Y. Sone, H. Sugimoto, Knudsen compressor, J. Vac. Soc. Jpn. 45 (2002) 138–141.
[15] Y. Sone, H. Sugimoto, Vacuum pump without a moving part and its performance, in: A.D. Ketsdever, E.P. Muntz (Eds.), Rarefied Gas Dynamics, AIP, New York, 2003, pp. 1041–1048.
[16] K. Aoki, P. Degond, Homogenization of a flow in a periodic channel of small section, Multiscale Model. Simul. 1 (2003) 304–334.
[17] H. Sugimoto, Y. Sone, Vacuum pump without a moving part driven by thermal edge flow, in: M. Capitelli (Ed.), Rarefied Gas Dynamics, AIP, New York, 2005, pp. 168–173.
[18] K. Aoki, P. Degond, S. Takata, Fluid-dynamic models for Knudsen compressors, in preparation.
[19] Y. Sone, Kinetic Theory and Fluid Dynamics, Birkhäuser, Boston, 2002.
[20] K. Aoki, Y. Sone, N. Masukawa, A rarefied gas flow induced by a temperature field, in: J. Harvey, G. Lord (Eds.), Rarefied Gas Dynamics, Oxford University Press, Oxford, 1995, pp. 35–41.
[21] Y. Sone, M. Yoshimoto, Demonstration of a rarefied gas flow induced near the edge of a uniformly heated plate, Phys. Fluids 9 (1997) 3530–3534.
[22] S. Kosuge, K. Sato, S. Takata, K. Aoki, Flows of a binary mixture of rarefied gases between two parallel plates, in: M. Capitelli (Ed.), Rarefied Gas Dynamics, AIP, New York, 2005, pp. 150–155.
[23] F. Sharipov, D. Kalempa, Gaseous mixture flow through a long tube at arbitrary Knudsen numbers, J. Vac. Sci. Technol. A 20 (2002) 814–822.
[24] M. Kayashima, Device for the transport and compression of gases by the use of the porous media, Patent JP. 1513106, B (in Japanese).
[25] S. Fukui, R. Kaneko, Analysis of ultra-thin gas film lubrication based on linearized Boltzmann equation including thermal creep flow, J. Tribol. 110 (1988) 253–262.
[26] F. Sharipov, Rarefied gas flow through a long tube at any temperature ratio, J. Vac. Sci. Technol. A 14 (1996) 2627–2635.
[27] C. Shen, Use of the degenerated Reynolds equation in solving the microchannel flow problem, Phys. Fluids 17 (2005) 046101.
[28] C. Cercignani, M. Lampis, S. Lorenzani, Flow of a rarefied gas between parallel and almost parallel plates, in: M. Capitelli (Ed.), Rarefied Gas Dynamics, AIP, New York, 2005, pp. 719–724.
[29] Y. Sone, Molecular Gas Dynamics, Birkhäuser, Boston, in press.
[30] T. von Karman, From Low-Speed Aerodynamics to Astronautics, Pergamon Press, Oxford, 1963.
[31] P. Charrier, B. Dubroca, Asymptotic transport models for heat and mass transfer in reactive porous media, Multiscale Model. Simul. 2 (2003) 124–157.
[32] K. Aoki, C. Bardos, S. Takata, Knudsen layer for gas mixtures, J. Stat. Phys. 112 (2003) 629–655.
[33] C. Cercignani, Plane Poiseuille flow and Knudsen minimum effect, in: J.A. Laurmann (Ed.), Rarefied Gas Dynamics, vol. II, Academic Press, New York, 1963, pp. 92–101.
[34] C. Cercignani, Plane Poiseuille flow according to the method of elementary solutions, J. Math. Anal. Appl. 12 (1965) 254–262.
[35] H. Niimi, Thermal creep flow of rarefied gas between two parallel plates, J. Phys. Soc. Jpn. 30 (1971) 572–574.
[36] C. Börgers, C. Greengard, E. Thomann, The diffusion limit of free molecular flow in thin plane channels, SIAM J. Appl. Math. 52 (1992) 1057–1075.
[37] F. Golse, Anomalous diffusion limit for the Knudsen gas, Asymptotic Anal. 17 (1998) 1–12.
[38] H. Babovsky, On Knudsen flows within thin tubes, J. Stat. Phys. 44 (1986) 865–878.
[39] H. Babovsky, C. Bardos, T. Platkowski, Diffusion approximation for a Knudsen gas in a thin domain with accommodation on the boundary, Asymptotic Anal. 3 (1991) 265–289.
[40] G.A. Bird, Molecular Gas Dynamics, Oxford University Press, Oxford, 1976.
[41] G.A. Bird, Molecular Gas Dynamics and the Direct Simulation of Gas Flows, Oxford University Press, Oxford, 1994.
[42] T. Ohwada, Y. Sone, K. Aoki, Numerical analysis of the Poiseuille and thermal transpiration flows between two parallel plates on the basis of the Boltzmann equation for hard-sphere molecules, Phys. Fluids A 1 (1989) 2042–2049; Erratum, Phys. Fluids A 2 (1990) 639.
[43] F.J. McCormack, Construction of linearized kinetic models for gaseous mixtures and molecular gases, Phys. Fluids 16 (1973) 2095–2105.
[44] B.B. Hamel, Kinetic model for binary gas mixtures, Phys. Fluids 8 (1965) 418–425.
[45] S. Chapman, T.G. Cowling, The Mathematical Theory of Non-Uniform Gases, third ed., Cambridge University Press, Cambridge, 1995.
[46] R.B. Bird, W.E. Stewart, E.N. Lightfoot, Transport Phenomena, John Wiley & Sons, New York, 1960.
[47] W.G. Vincenti, C.H. Kruger Jr., Introduction to Physical Gas Dynamics, John Wiley & Sons, New York, 1965.

[48] C. Cercignani, Rarefied Gas Dynamics, From Basic Concepts to Actual Calculations, Cambridge University Press, Cambridge, 2000.
[49] Y. Sone, Asymptotic theory of flow of rarefied gas over a smooth boundary I, in: L. Trilling, H.Y. Wachman (Eds.), Rarefied Gas Dynamics, vol. 1, Academic Press, New York, 1969, pp. 243–253.
[50] Y. Sone, Asymptotic theory of a steady flow of a rarefied gas past bodies for small Knudsen numbers, in: R. Gatignol, Soubbaramayer (Eds.), Advances in Kinetic Theory and Continuum Mechanics, Springer-Verlag, Berlin, 1991, pp. 19–31.
[51] C. Cercignani, F. Sharipov, Gaseous mixture slit flow at intermediate Knudsen numbers, Phys. Fluids A 4 (1992) 1283–1289.